Juha Haikola

Wear-resistant embedded thermal sensor

School of Electrical Engineering

Thesis submitted for examination for the degree of Master of Science in Technology.

Espoo 18.4.2012

Thesis supervisor:

Prof. Ilkka Tittonen

Thesis instructor:

M.Sc. (Tech.) Sanna Tervakangas

Aalto University
School of Electrical
Engineering

AALTO UNIVERSITY
SCHOOL OF ELECTRICAL ENGINEERING

ABSTRACT OF THE
MASTER'S THESIS

Author: Juha Haikola

Title: Wear-resistant embedded thermal sensor

Date: 18.4.2012 Language: English Number of pages:6+56

Department of micro- and nanosciences

Professorship: Electrophysics Code: S-129

Supervisor: Prof. Ilkka Tittonen

Instructor: M.Sc. (Tech.) Sanna Tervakangas

The work reported in this thesis has been carried out as a part of Intelligent and customised tooling (IC2) EU project, aimed at developing embedded sensors onto surface of industrial tools. To this end, the amorphous carbon thin films fabricated primarily on alumina and insulated steel substrates using DIARC FCAD method are inspected for thermistor properties. In order to embed this sensor on an industrial tool, the possible disturbances from industrial environment were examined along with other parts of the device.

As a result, the thermistor behaviour following the hopping conductivity mechanism has been observed between room temperature and 250 ℃ on both substrates. In addition, the material was found to possess a piezoresistive behaviour, although, this behaviour was small compared to the overall temperature sensitivity.

Keywords: Thermistor, Amorphous carbon, Resistance, Temperature, Piezoresistivity, Hopping conductivity, Thin film, Embedded structure, Sensor

AALTO-YLIOPISTO
SÄHKÖTEKNIIKAN KORKEAKOULU

DIPLOMITYÖN
TIIVISTELMÄ

Tekijä: Juha Haikola

Työn nimi: Kulutusta kestävä integroitu lämpötilasensori

Päivämäärä: 18.4.2012 Kieli: Englanti Sivumäärä:6+56

Mikro- ja nanotekniikan laitos

Professuuri: Sähköfysiikka Koodi: S-129

Valvoja: Prof. Ilkka Tittonen

Ohjaaja: DI Sanna Tervakangas

Diplomityö on tehty osana Intelligent and customised tooling (IC2) EU-hanketta, jonka tarkoituksena on integroitujen sensoreiden valmistaminen upotettuina teollisten koneen osien pintoihin. Tässä työssä tutkittiin amorfisesta hiilestä DIARC FCAD-menetelmällä valmistettuja ohutkalvoja termistoriominaisuuksien määrittämiseksi alumiinioksidi- ja eristetyillä terässubstraateilla. Myös materiaalin mahdollisia pietsoresistiivisiä ominaisuuksia tutkittiin teollisen ympäristön aiheuttamien häiriöiden varalta.

Termistorin havaittiin seuraavan hopping conductivity- mallia huoneenlämmön ja 250 ℃ välillä molemmilla alusmateriaaleilla. Lisäksi materiaalin todettiin käyttäytyvän pietsoresistiivisten materiaalien tavoin. Termistorin lämpötilaherkkyyden todettiin tosin olevan huomattavasti merkittävämpi rakenteen resistanssiin vaikuttava tekijä.

Avainsanat: Termistori, Amorfinen hiili, Resistanssi, Lämpötila, Pietsoresistiivisyys, Ohut kalvo, Integroitu rakenne, Sensori

Contents

Symbols and abbreviations

a-C	Amorphous carbon
FCAD	Filtered cathodic arc deposition
IC2	Intelligent and customised tooling, an EU project
NTC	Negative temperature coefficient
PTC	Positive temperature coefficient
ta-C	Tetrahedral amorphous carbon

1 Introduction

The master's thesis is done as a part of an EU project IC2, intelligent and customized tooling. This part of the IC2 project concerns essentially the development of wear-resistant coating of industrial tooling embedded with sensing structures. These intelligent tools can increase the durability of tools and also enhance the control over the fabrication parameters in industrial processes.

The aim of this thesis is to develop a thermistor device and to embed this on the surface of an insulated steel substrate under a wear-resistant coating. For fabricating such a device, this thesis strives to utilize the exceptional physical properties of the diamond like amorphous carbon. The different amorphous carbon based materials fabricated have been under a tremendous research effort, not only because of the physical properties, but also because of the semiconducting behaviour reported in recent studies. These properties differ from those observed in conventional, crystalline semiconductors, because of the amorphous nature of the material. [1–3]

The semiconductors being inherently thermistors enable almost the whole device being completely fabricated from amorphous carbon, apart from contacts and insulation. This also makes it easier to fabricate the device as many issues related to the adhesion are not present due to a low number of different materials used in the structure. However, the properties of amorphous carbon depend significantly on the specific fabrication method [1]. Thus, the main effort in this thesis is directed into the characterisation of the thermistor behaviour of the specific amorphous carbon films fabricated with the DIARC FCAD method. This method essentially is deposition process using a filtered cathodic arc in a vacuum at temperatures close to the room temperature.

In addition to describe the thermistor properties, three other aspects related to the goals of the project are included in this thesis. At first, the sensor is inspected for the effects caused by a protective amorphous carbon coating fabricated as the topmost layer. Secondly, the piezoresistive effects are examined as the sensor is intended to be operated in industrial applications. Thirdly, several dielectric layers are inspected for providing insulation for the structures fabricated on the steel substrate. Furthermore, three different masking methods are compared in order to develop the actual patterned structures.

This thesis is organised as follows. The section 2 begins with the theoretical description of semiconductors, thermistors and amorphous carbon, with more detailed discussion that is deemed of importance in terms of electrical and semiconducting properties. This is continued in section 3 with the description of experiments conducted regarding the fabrication of the device based on amorphous carbon and analysis of the material properties. Section 4 presents and discusses about the results achieved through the experiments. The section 5 present conclusion of this work. The section 6 gives a short outlook based on the most interesting results and experience gained in this thesis.

2 Theory

This section aims at providing sufficient theoretical understanding for the properties of amorphous carbon related to thermistor applications. The section begins with a general description of material properties. Additionally, the principles of semiconductors, semiconduction as thermistors and semiconductor-metal contacts are discussed. The section is finished with a theoretical introduction to amorphous carbon with special emphasis on electrical properties. This contains a description on how the conductivity is altered by the amorphous nature of the material and by doping in order to modify the electrical properties. Also, annealing of the material is considered as this affects the structure of the fabricated network.

2.1 Some aspects of solid state physics

It would be impossible to describe properly theories behind the device operation based on semiconducting materials without a general view on solid-states physics. This part gives an introduction to the crystalline solids, whereas amorphous materials are discussed later. There is also discussion on the general level of amorphous structure and phenomena such as electrical conductivity, defects and adhesion of different material layers.

Most solid materials are described by a periodic crystalline lattice. The periodicity results in the smallest possible structure, a unit cell, which cannot be divided into smaller periodic structures. Depending on the number of different atoms in the structure and their physical properties, the atoms in the unit cell obtain different spatial arrangements. For mathematical convenience, the lattice is considered to be formed by infinitely repeated unit cells. The infinity is a reasonable assumption because the vast amount of atoms contained in macroscopic samples.

The amorphous structure does not follow the periodic lattice. It can rather be understood as a network with varying atomic distances and angles. However, the amorphous network has highly correlated atomic separations and angles between atoms over short distances. This correlation causes the structure to be close to the periodic one in small volumes, thus in this aspect it possesses similarity with crystalline structure. On the other hand, the amorphous material lacks long range order. This allows different parts of the amorphous network to be significantly different, and the network to have random nature.

The periodic structure of crystalline materials leads to an electronic band structure, which can be used to solve the material properties depending on the electronic configuration. The band structure is obtained from the dispersion relation of electrons and the Fermi distribution. These are combined for a material specific distribution of electrons in the allowed energy states. These energies are, depending on the lattice and material, generally divided in two bands separated by a gap in which electrons have no allowed energies. The short range order of amorphous materials results in a fairly unchanged band structure.

Another dispersion relation exists for lattice vibrations, phonons, which also affects the material properties. In other words, the phonons represent atoms vibrating

around their site in the lattice and the scattering of these vibrations through the lattice. Along with electrons, phonons contribute significantly to thermal and electrical conductivity and other properties of solids.

In principle, the electrical conduction in a material is the result of an electric field affecting electrons. The states occupied by electrons are imbalanced in the band structure resulting in more electrons travelling in a direction determined by the electric field. In case where the band is fully occupied by electrons, they can not be imbalanced in the structure and thus the fully occupied band does not contribute to conduction. Additionally, the conduction is hindered by electron dynamics due to several reasons, such as electron-electron scattering and by interaction with phonons or defects in the lattice.

In solids, a lattice or a network can contain defects. These affect the material properties. In amorphous carbon their presence is different from the crystalline structure, though their role in the properties of amorphous carbon requires including them in theoretical discussion.

In general, defects can be individual grains, planes or 1D or 0D objects. Though the first three types of defects affect the mechanical properties, the point defects can change the electrical properties of the material. There can be several different kinds of point defects though the most common ones are vacancies, interstitials and impurities. The vacancies are sites in the lattice that are not occupied by atoms. These vacancies are supported by the crystalline structure. The interstitials are atoms that are located in between the sites determined by the lattice. The impurities are atoms different from the main elements occupying the lattice. The atoms with the same electronic configuration as the main atoms would not cause much difference, but atoms of different group either capture an electron from the lattice or release it into the material. Thus in a short range, these atoms contain different electric charge from the rest of the lattice causing an increase in electron scattering. In general, most defects cause this kind of effect, though the largest effect is caused by the impurities of different electronic charges. Additionally, for specific materials, the structure may contain atoms with dangling bonds. These atoms do not have covalent bonds with all its electrons and some of these are thus unbounded causing them to effectively trap electrons disturbing conductivity.

In this thesis the samples consist of different thin film layers on top of a substrate. One aspect relates to the layers of different materials in a sense how and if they are adhered to each other on the microscopic level. In general, there are two issues on the microscopic level that affect the adhesion between different materials. The first one is the ability of different elements to bond together. This depends on their respective electrical configurations. If the bond strength is not clearly higher than in the unbound situation, then thermal energy typically causes breaking of the bonds and the overall structure.

One more issue is related to the structures of both materials. If the separation between atoms or if the typical lattices that the material form of differ sufficiently from separate layers, there may occur problems. In the junction between two materials these differences cause atoms to adapt to another kind of structure, which causes stress within the material. In essence, this stress results in a rise in the energy

required to bond the structure.

2.2 Semiconductors

This thesis deals with the properties of semiconducting amorphous carbon thin films. The nature of semiconductors is therefore described in a more accurate fashion. At first, some properties of conduction processes in a semiconductor material are introduced. Secondly, the temperature dependency of conduction is discussed separately as the semiconductors are innately thermistors, which is the important basis for this thesis. Thirdly, the metal-semiconductor contact is described. These contacts exist in the structures fabricated and examined in this thesis.

As noted, the Fermi distribution defines, in part, the band structure of the material. The Fermi distribution leads to a cut-off energy, Fermi level, that describes the maximum energy, that the most energetic electrons can have at absolute zero temperature. The distribution suggests that then all states below the Fermi level are fully occupied and respectively unoccupied above this level. This energy in reference to the bond energies affects the conduction of the material as fully occupied bands do not contribute to conduction. If the Fermi level is located in the gap region between two bands, no conduction occurs in the material, at least at zero temperature. The metals have the Fermi level within the band of allowed energies, resulting in excellent electrical conductivity. In case where the Fermi level is located in the band gap region, the width of the gap, the band gap energy, divides these materials into semiconductors and insulators. Though no definite value for the gap size separates these two categories, the semiconductors possess considerably smaller forbidden energy gap.

At nonzero temperature some electron become excited above the Fermi level. The energy that enables the conduction by electronic excitations to the conduction band is called the activation energy. The band below the Fermi level, valence band, on other hand has lost electrons to the conduction band. The bands are now only partly occupied and contributing to the electrical conductivity. However, on the valence band, the conduction is typically described as conduction of holes, or the lack of electrons of an almost completely occupied band. The semiconductors are thus further classified by the type of charges having the largest effect on conduction, as the result of the Fermi level located closer to either band. These are called either n-type or p-type semiconductors for the electron or the hole conductivity, respectively.

In semiconductors, the conductivity can be altered by adding dopant atoms as impurities in the structure. These provide additional electrons to the conduction band for conduction, when impurity has additional electrons to contribute and is energetically close to the conduction band, or in the opposite case capturing electrons from valence band and creating holes. The location of the dopant atoms energy with respect to the Fermi level of the semiconducting material is decisive, whether dopant acts as a donor or an acceptor, respectively. In general, good dopants are located fairly close to either band. Also the effectiveness of the doping atom is important, meaning the amount of dopant atoms contributing to the conductivity.

2.2.1 Thermistor

In order to discuss the thermistor properties of amorphous carbon structures, it is necessary to define this kind of device. This section describes the theory behind the thermistor, a material that changes resistance according to the temperature. We consider the general principles of resistance-temperature behaviour and specifically look at the suitability of using semiconductors as thermistors. Also various models for thermistor behaviour are shortly previewed of amorphous carbon structures fabricated for this thesis.

Two different kinds of behaviour can be observed, either the resistance increases or decreases with rising temperature. These two alternatives are called the positive and negative temperature coefficient (PTC) and (NTC) thermistors. The former ones consist mainly of metals, whose conductivity is determined almost explicitly by the lattice vibrations. The phonons interact with travelling electrons by scattering, causing electrons to alter course and velocity randomly. Thus the electronic mean free path decreases with the increasing the number of phonons, essentially meaning that electrons are affected by electric field for shorter period and travel shorter distances between the scattering events. Consequently, the resistance of the material follows the density of phonons, which increases along with the temperature.

The latter, NTC, possesses different origin. The increasing temperature leads to an increase in the level of conductivity in semiconducting material through the extended states by thermal excitation of electrons from the valence to the conduction band. The occupation in these bands by holes or electrons follows roughly an exponential distribution as a function of temperature. Naturally, the phonons have a similar effect on electron scattering as in metallic materials, yet the increase in the number of conducting electrons is so significant that the phonons cause only a minor disturbance, when compared to metals with initially low resistance.

In this thesis, the thermistor is fabricated from amorphous material. As later discussed, the conduction in an amorphous carbon differs from the conductivity defined by extended states as conduction is observed also below activation energy. The model for conventional semiconducting thermistor can be invalid for an amorphous thermistor, at least in a part of the temperature range. The exponential relation between resistance and inverse temperature is

$$R = Aexp(B/T), \tag{1}$$

where A relates to the level of resistance at specified temperature (typically room temperature) and B to the slope at which resistance decreases. The resistance of amorphous semiconducting material follows variable range hopping conductivity at low temperatures [2]. In mathematical form, the resistance of the material changes according to the hopping conductivity model as

$$R = Aexp(B/T^{1/d+1}). \tag{2}$$

The parameter d depicts the dimensionality of the structure, A and B are parameters that are related to resistive behaviour, as in equation 1.

The hopping conductivity is explained more thoroughly together with other properties of amorphous carbon. The matter of immediate interest is the switching temperature between the two conduction mechanisms. The major problem that might arise is related to the switching temperature being located in the vicinity of the temperature range being measured. Being the case, the resistance of amorphous carbon would change with temperature by both conduction methods, making the modelling remarkably difficult. According to several experiments, the conduction mechanism of amorphous carbon is reported to switch from hopping conductivity to actual conduction between extended states in the temperature range of 350–380 K (80–110 ℃) [4, 5]. Yet, differently fabricated amorphous carbon materials have remarkably varying properties, which include the activation of the extended states conductivity. As several simulations have predicted, the hopping conductivity can be a major contributor even up to 500 K (230 ℃) temperature [6].

2.2.2 Metal-Semiconductor junction

For this thesis the nature of the junction between semiconducting and metallic material needs to be described. This is relevant as the structure under study is semiconducting while the measurements are made using metallic contact layers.

In principle the junction between metal and semiconductor can be either an ohmic or a so called Schottky contact. This depends on the width of the band gap of the semiconductor and the Fermi levels of both materials. In case of an ohmic contact, the current through the junction is linearly dependent on the voltage over the junction, whereas the Schottky contact is essentially a diode allowing current effectively only in one direction.

In general the semiconductors form a space charge region when they are in contact with other materials. This region forms when free charges on both materials gather to the junction, depending on the difference in the Fermi energies of both materials. The movement of charges balances the system to a state, in which the electric field induced by the gathered charges on the surfaces of metal and semiconductor balance the initial difference in the Fermi energies. In case of the metal-semiconductor junction, on the metal side the region showing accumulated charging is extremely narrow as a result of excellent conductivity. This results in no significant alteration of the electrical behaviour of the metal. On the semiconductor side, the charged region is wider. This causes the electric field of the charged region on the semiconductor side to decrease gradually. This gradual change also affects the band structure, which locally bends with respect to the charge on the semiconductor side.

Depending how the band is bent, the structure might act as a barrier for charges on the metal side. However, the transport of charges from the semiconductor side is allowed as a result of gradually rising slope. This is essentially the nature of a Schottky barrier. However, two cases allow also an ohmic contact between metal and semiconductor. In the first case, the bending of the conduction band can enable a direct highly conductive contact in the junction. In other case, the charge on the semiconductor side is concentrated on a sufficiently narrow volume. This narrow

region allows tunnelling of electrons through the potential barrier, creating current on the junction that is significant in both directions.

Amorphous carbon provides even further possibilities for ohmic contact with certain materials. During fabrication these metals form carbides on the junction. This carbide region can be considered as a gradual change between carbon and metal. However, the nature of this region is unclear, yet several studies have proven that the low resistance carbide layer generates ohmic contact between amorphous carbon and several different metals, such as titanium [7, 8].

2.3 Amorphous carbon

In this section, several aspects of amorphous carbon are discussed in general. The section begins with the classification of different amorphous carbon materials. Secondly, a brief discussion is included about the band structure of amorphous carbon with respect to crystalline counterparts, diamond and graphite. This is continued with a separate discussion considering the differencies in the structures caused by the localised states and the resulting hopping conduction. In addition, there is discussion regarding doping and the thermal annealing of the amorphous structure and the respective effects in the material properties.

Carbon atoms are capable to form crystalline lattice with two different bondings, sp^2 or sp^3. The latter corresponds to a lattice where each carbon atom forms four strong σ bonds with other carbon atoms, resulting in a diamond lattice and namely in diamond as a macroscopic material. In the former, one of these strong bonds is replaced by a weaker π bond whereas other bonds are on the same plane. This results in strong sheets of carbon connected by the weaker bonds, as in graphite.

In amorphous material both of these bonds can coexist more naturally as the result of a varying network. Actually, the fraction of sp^3 bonds is used to classify different amorphous carbon materials. The amorphous carbon network containing large fraction of sp^3 bonds possess physical properties similar to diamond. The two major types are amorphous carbon and tetrahedral amorphous carbon, ta-C, for the majority of either sp^2 or sp^3 bonds respectively. Additionally, in amorphous carbon the third type of bond, sp^1, is also possible. This bond begins to exist in significant amounts only after incorporation of hydrogen or nitrogen into the carbon network. Figure 1 illustrates ternary phase diagram describing this division of amorphous carbon structures depending of atomic bonds present in the structure. In general, the mechanical properties such as elastic modulus, internal stress, hardness and density are maximal on the top corner, whereas the electrical properties are maximal on the bottom left corner. The internal stress is actually a result of metastable configuration of the sp^3 network and alters into sp^2 network when possible, as during annealing. [1]

In essence, the form of the amorphous carbon band structure is an intermediate between the diamond and graphite band structures. As in figure 2, the σ bonds of the sp^3 network are as in diamond with large band gap and the π bonds of the sp^2 are contained within the band gap of these diamond like bands [1]. Though, there is an additional, major difference due to the disordered nature of amorphous structure.

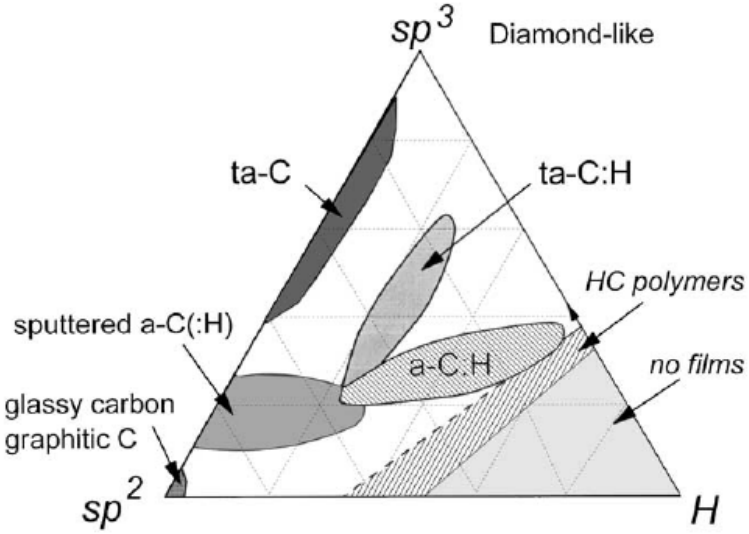

Figure 1: Ternary phase diagram classifying the amorphous carbons by the different bonds in the network. [1]

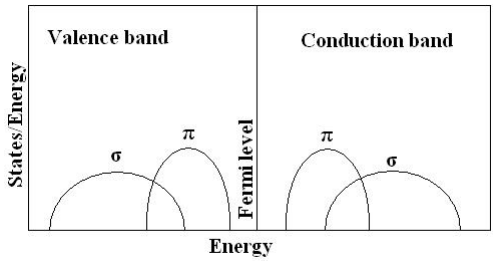

Figure 2: The scheme of the band structure of amorphous carbon as a composition of the σ and π band structures of diamond and graphite.

This disorder causes localised states to emerge in significant numbers in the amorphous materials affecting the electrical properties. These localised states are physically separated, thus essentially working as traps for conducting electrons. However, with sufficient excitations the electrons may move from these states either to extended or, with less effort, to other physically nearby localised states. Anyway, these excitations result in weaker hopping conductivity with respect to the conductivity of metallic or extended states.

2.3.1 Localized states and hopping conductivity

In amorphous materials, similar conduction mechanisms take place as in metal and in semiconductors. In amorphous carbon, which is a semiconductor, similar thermally activated conduction through the extended states can take place, as in crystalline semiconductors. In addition, the structure in the amorphous carbon causes

additional energy states to emerge in the gap region. The gap is filled by localised states near the band edges as well as the defect states in the mid gap region, which contribute to conduction in an interesting fashion. Before discussing the effect on conductivity, the localised states are described for their nature and the change they cause to the amorphous band structure.

The nature of the extended and localized states is certainly a significant factor in amorphous carbon. The extended states exist uniformly in the material. In other words, due to sheer amount of these states, they are reachable by electrons regardless of their physical location in the material, assuming the states are not already occupied and the electron receives sufficient energy.

Each localised state is confined into a small spatial region in the material, effectively separating the localised electrons from the rest of the material. For their different nature, the localised states in the mobility gap region of amorphous semiconductors are divided between the band tail and defect states. In amorphous carbon, the sp^2 clusters confined in the sp^3 network are separated from each other, which effectively results in localisation. The cluster sizes and shapes have vary, which also causes variation in respective localised energy states. This results in localised states distributed through the mid gap region.

The localised band tails depend significantly on the sp^2 structure in the network, which results from the fabrication method. The variation with different fabrication methods causes significant differences in the localised states. This can be seen in figure 3 with the density of states and inverse participation ratio calculations for amorphous carbon materials with different sp^3 content by [9]. For instance, the hydrogenated amorphous carbon has remarkably long tails, because of large variety of clusters, whose energy states overlap over the mid gap and mix together with the defect states [1]. On the opposite end is a ta-C structure with a low sp^2 content and small clusters, where the π bands can entirely be localised and possess sharper tails [5].

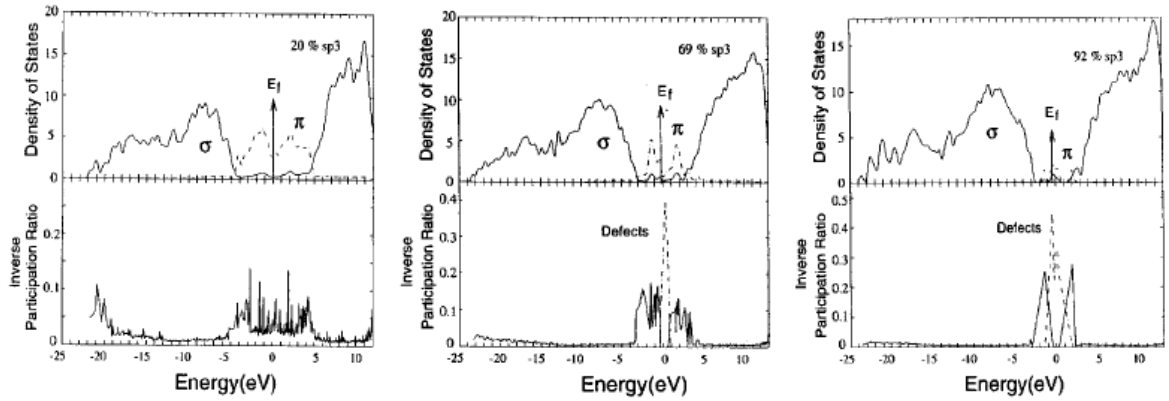

Figure 3: The calculated densities of states and inverse participation ratios represent the different level of localisation in amorphous carbon materials with different sp^3 content. [9]

The defects are of different nature in amorphous materials, as there is no crys-

talline lattice and thus the network cannot have similar structural distortions. By definition for the amorphous networks, the defect corresponds to a configuration different from the main part of the network. Additionally, the defects are defined to correspond mostly to states near the Fermi level in the mid gap region, as the other cluster configurations are mostly band tail states. The defects effectively affecting are those states with only a single occupying electron. In amorphous carbon such defect states are mostly caused by the dangling bonds and clusters with an odd number of sp^2 sites. The latter is further affected by the composition of the cluster and the level of its distortion. [1, 10]

In the band model related to the crystalline semiconductors, and metals and insulators, the bands are typically composed of extended states. The other states are typically considered as defects as they are localised and affect the properties in only a small region. Yet, in amorphous materials, especially in those with multiple bonding types, the bands can consist of significant amount of these localised states. The amount of these localised states caused a part of them function as extended states, taken that there is sufficient density of these states on a specific energy. This essentially means that the material possess physically dense network of these normally localised states, which are essentially extended through the material. Thus there exist an energy, referred as the mobility edge, on both valence and conduction bands, which separates the localised states with sufficient amount to form a continuum through the material. Even though there still exists a large number of states contained between the mobility edges, these states are localised to such extent that they cannot contribute to the electrical properties of the material similarly as is the case with extended states. This mobility gap effectively works as the band gap of the crystalline materials, though not affecting the optical properties of the material in same extent. Instead, the optical gap is separately defined as unaffected by the localisation and thus narrower than mobility gap in amorphous carbon. Figure 4 schemes the localised band tail and defect sites in the mobility gap. [2, 11]

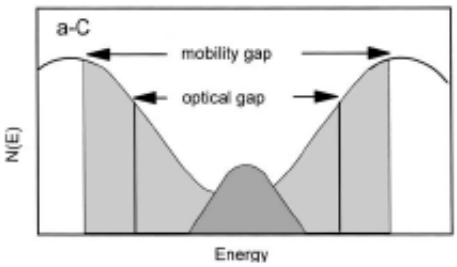

Figure 4: The scheme of the density of states of amorphous carbon. The localised band tail and defects sites are located within the mobility gap. The optical gap in amorphous carbon is narrower than mobility gap as this is not affected by the localisation of the states. [1]

The localised states contribute to conduction beginning on relatively low temperatures, compared to the conduction by extended states. The electrons can traverse the network by hopping between the localised states in the mobility gap before the

conduction through extended states is thermally activated. This process is essentially an interaction between phonons and electrons in the localised states. [2]

It has been suggested that there are separate phases for hopping conductivity between the defects of the network located in the mid gap region and between the localised band tails. The former would be mainly induced by the phonons, where lattice vibrations transfer energy between the electrons in the localised states. The latter is more direct hopping, or tunnelling, between the nearest neighbour π states. These two methods are typically hard to separate as a result of the partial overlap of the band tails and mid gap defects states. Thus observing them separately requires a sufficiently low sp^2 content. [5]

In the end, there are three different conduction methods possible in amorphous carbon. These are each thermally activated at different temperatures, first one is the nearest neighbour hopping, then the band tail hopping and finally the extended states conductivity.

2.3.2 Doping of amorphous carbon

In order to be of any significant use as a semiconductor, the doping of the material is expected to affect the electrical and optical properties of the material. For amorphous carbon several elements have been intensively studied in this respect. Nitrogen is probably the most studied dopant for amorphous carbon. Also, hydrogen is widely studied though it does not act as a dopant for semiconducting purposes, but rather compensates dangling bonds within the network. Yet, there are other elements that have been studied for doping purposes, such as n-type dopant phosphorous and a p-type boron. However, all dopants are argued not to effectively dope amorphous carbon in the sense of conventional semiconducting material, where doping affects the location of the Fermi level.

It was initially reported, that ta-C can be doped to n-type with incorporation of phosphorus [12]. Similarly the p-type dopant, boron, has been successfully incorporated into ta-C structure [13]. The subsequent studies of the n-type dopants introduced nitrogen, which was expected to function better than phosphorus as the result of the similar atomic size between nitrogen and carbon [14]. All three doping elements show clear decrease in resistivity, from the initial of 10 $M\Omega cm$ value to approximately 10 Ωcm. However, later studies show an initial increase in the resistance and activation energy for nitrogen doped samples [14, 15]. This can be associated to the rising Fermi level passing the center of the mobility gap. This is based on the knowledge that ta-C has inherently the Fermi level slightly below the middle of the gap corresponding to a p-type semiconductor. This also means that nitrogen functions as an n-type dopant for amorphous carbon. Nitrogen incorporation has very complex effect on both Fermi level and conductivity, instead of simply substituting carbon atoms in the amorphous sp^3 lattice [14]. Results suggesting p-type doping with boron have also been reported, based on the decreasing activation energy and increased conductivity [13, 16].

There have been results indicating changes on amorphous carbon structure as a result of doping. In essence, this is observed by a decrease in the stress in the

structure and corresponding decrease of the sp^3 content of the network. These structural changes significantly affect the electrical properties of ta-C. The effect that the doping has on conductivity, and presumably with the Fermi level location, relates to several structural changes. The doping increases conductivity of the ta-C structure. This is, however, only partly due to substitutional doping of sp^3 sites, which causes the major movement of the Fermi level. The dopants, with their Fermi levels overlapping the π bands of the amorphous carbon, are more likely to affect graphite structures of ta-C, which affects the localised states of the network. This in turn plays a considerable role in conductivity and the location of Fermi level. [3, 10, 17–19]

The initial theory for the effect of the nitrogen doping on ta-C was provided by Robertson and Davis [3], in an attempt to produce C_3N_4 compound lattice that is presumably harder than diamond. It has been stated that doping of nitrogen could, in addition to the substitution of carbon atoms in the lattice and maintaining sp^3 structure, cause non-doping substitution or substitution in graphitic sp^2 clusters. The figure 5 represents different bonding configurations that the nitrogen can obtain in amorphous carbon structure. The non-doping substitutions can partly explain the weak doping efficiency, which is roughly 1 % of nitrogen in ta-C, which in turn is generally common in amorphous semiconductors. The other reason is that in the case of substitutional doping, either sp^3 or sp^2, there is a tendency for an electron contributed by nitrogen substitution to compensate for the defect state near mid gap region, thus providing a lesser effect in the location of the Fermi level. The non-doping substitutions additionally affect the conductivity of the structure as they tend to increase the localised states in the mid gap region. This effectively increases the amount of electrons contributing to the hopping conductivity. In addition, the increased amount of the states in the π bands results in the change of location of the band and mobility gap, causing observed effects in decreasing optical gap and partly affecting the conductivity. [3, 18–20]

Another method of affecting the properties of amorphous carbon is the hydrogen incorporation. This in principle does not affect the Fermi level, but is instead expected to compensate for the defect states in the mobility gap as in amorphous silicon. However, it has been suggested that hydrogen is most likely to bond with the sp^2 sites in the network. Furthermore, hydrogen is assumed to be trapped within the network unbound rather than compensate the dangling bonds. This effectively causes an increase in resistivity and respective optical and electric properties, along with increasing sp^3 content. This has been seen to occur with small amounts of hydrogen incorporated to the amorphous carbon structure. In larger doses, the opposite effect starts to take place. This has been suggested as the result of destabilization of the carbon network, which reverts to sp^2 ruled network. [9, 21]

2.3.3 Annealing amorphous carbon

The annealing of amorphous carbon has been studied for any structural changes towards more stable sp^2 ordering of the network and also to decrease an internal stress within the network. The annealing of structure provides energy to the net-

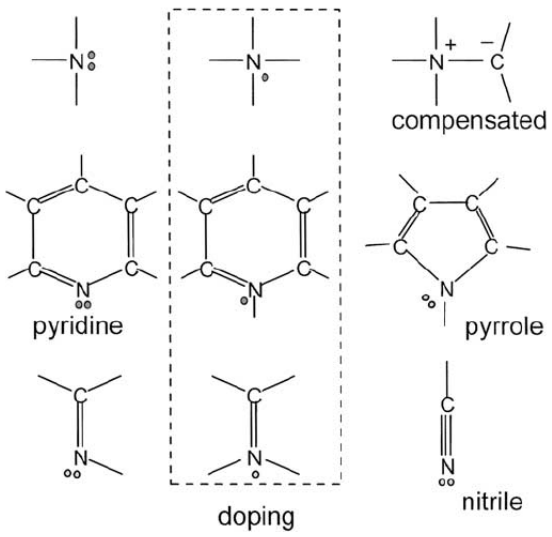

Figure 5: Several different bonding configurations that the nitrogen can adopt in the amorphous carbon network. The dots present non-bound electrons. These different configurations, of which only several actual dope the material, cause a decrease in the doping efficiency. [1]

work, which enables it to reorganize into a more stable configuration.

The tetrahedral amorphous carbon maintains its structure without distortion when annealed in temperatures up to 600–700 ℃ in vacuum. Only after this temperature sp^3 content starts to decrease and the optical gap to close slightly before collapse at around 1100 ℃. In atmospheric conditions, amorphous carbon was found to oxidise in temperatures of roughly 450–500 ℃. However, increase in conductivity is observed even below this temperature range, suggesting the reorganisation of the network. This reorganisation essentially concerns the sp^2 sites, whose amount is not dramatically increased, thus resulting mainly in single sites contained within the network. Yet, these sites provide increased amount of hopping centres causing exponential increase in conductivity. At temperatures near 600 ℃, the clustering begins to take place, which results in the decrease of the optical gap rapidly decreasing resistivity. Relaxation also provides considerable relief in compressive stress in the system, inherent to deposition process. [22, 23]

Similar yet thermally less stable effects, are observed in hydrogen or nitrogen doped ta-C. At 600 ℃ the structure begins to alter into sp^2 dominant network. However, a significant stress relief is observed at even lower temperatures indicating slowly increasing or reforming the sp^2 site content. Additionally, as the dopant atoms incorporated in the a-C network have different configurations of substitution having weakly bonded or merely interlocked atoms in the system. Thus annealing the structure causes interlocked dopant atoms to diffuse onto the surface and into the air. The higher the annealing temperature the more of the doping atoms in the structure are being affected. In case of the crystalline structure this would lead into vacancies in the structure, however, amorphous material is more likely to

collapse. [1, 24, 25]

McCulloch studied the annealing of the amorphous carbon of lesser sp^3 content. Even though sp^2 content similarly increased during annealing the graphite like structure occupied its preferred orientation perpendicular to the film surface. The increase of sp^2 content causes physical expansion of the structure as graphite like sp^2 is less dense than diamond like sp^3 structure. This causes the increase of stress in the structure, which is then partially compensated by orientation of graphite like sheets. [23, 26]

3 Experimental

The goal of this thesis was to develop a thermistor, which is based on the semiconducting properties of the thin film processes out of amorphous carbon. The first part of this section describes the samples used in these measurements. The second part illustrates the experiments conducted to study the thermistor behaviour and also the piezoresistive properties of the material.

3.1 Samples

The samples experimented in this thesis were generally tetrahedral amorphous carbon thin films masked into rectangular patterns. These were fabricated on varying planar substrates in order to accurately examine several different properties. In addition, the titanium thin film pads were fabricated overlapping these structures as contacts for electrical measurements.

This subsection illustrates the parts associated with samples and their fabrication. In the beginning, there is a discussion of the properties of four different substrates used and the particular reasons of using these. Secondly, the masking methods used in patterning the sample structures are described. Thirdly, the different structural layers are described along with the fabrication method. Finally, adhesion is discussed in terms of the experiments used in measuring this property.

3.1.1 Substrates

In this thesis, the thermistor sample structures were produced either on aluminium oxide (alumina), silicon, polymer or insulated steel substrate. The steel and alumina substrates were selected for the inspection of thermistor properties, whereas the polymer substrate was used as a more sensitive substrate for piezoresistivity measurements. Silicon was tested in initial phase of this thesis as an alternative smooth substrate for the fabrication of the structures.

The alumina substrate, containing 96 % of Al_2O_3, was used in a form of a square plate with 1 mm thickness. The alumina was selected for experiments due to the previous experience of well adhered amorphous carbon thin film layers fabricated on the substrate. Additionally, the thermistor is an electric device and thus the properties should initially be examined on an insulating substrate.

In comparing alumina substrate properties with other alternative materials, the largest difference is the roughness of the surface, varying in the range 0.2–0.8 microns. This roughness causes significant changes in several properties of the layer, most importantly an increase in the level of resistance. Another physical property that is of interest, is the elastic modulus of alumina, which is stated to be 330 GPa, which is of similar order as with amorphous carbon layers. Thus, alumina is considerably rigid, which in regard of piezoresisitivity measurements decreases the potential effect that the a-C thin film might possess.

Steel, labelled Orvar 1.2344, was another substrate material used in thermistor property measurements. Similarly to alumina, steel substrate samples were also

square shaped of similar area, but with thickness of 10 mm. This larger thickness limited the piezoresistive measurements conducted in this thesis, as the substrate could not be bent as easily as the thinner alumina. The roughness of the substrate was reported to be less than 0.05 microns, which is considerably smoother when compared with alumina. For the measurements of electrical properties on the steel substrate an insulating coating had to be fabricated before the sensing structure. However, these coatings were either very smooth after fabrication or were polished afterwards to match the roughness of the substrate, meaning that no significant change in the roughness is expected with insulating layers. These different insulating layers are considered in the end of this part.

Another substrate with low surface roughness, silicon, was used in initial experiments for fabricating the amorphous carbon sensor. Most importantly silicon worked as a general test substrate for masking methods along with alumina. In essence, the silicon was not much used in this thesis. A measurement for the resistivity of the titanium contacts was conducted on a silicon substrate for comparison between two substrates of different roughness.

Similarly less used substrate was the polymer, Grilamid TR 55 LX. With much lower elastic modulus of 1.9 GPa, this polymer provided much better measurements of the piezoresistive potential of the amorphous carbon thin films.

Finally considering the insulating layers fabricated on the steel substrate, for which purpose there were several layers under consideration. Two of them were thin films, whose thickness was less than 0.5 microns, fabricated with the DIARC FCAD method, an referred as layers I1 and I4. Two other layers were provided by external parties taking part in the IC2 project. First of these was an alumina layer with thickness of 5–10 microns and the second a composition of aluminium and magnesium oxide, spinel, with thickness 50–100 microns, corresponding to layers named I2 and I3, respectively.

Due to an insulating layer, the metal contacts could not be fabricated excessively large. The larger contacts would have increased the probability of overlapping a cavity on the insulating layer reaching the steel substrate. If there were such a cavity contact on both sides of the sensor, the sensor structure would be completely bypassed and the structure could not be used to measure temperature. This probability of fabricating titanium contact on a bore was examined by fabricating a large matrix of titanium square shaped samples with 1 mm and 3 mm sides on the insulating layer. Resistance between these squares and the steel substrate was then measured to characterise the amount and the quality of the contacts, with respect to the insulating capability of the layer. The resulting quantity of contacted squares is used to calculate the probability of contact through the insulating layer.

3.1.2 Masking

As a part of this thesis different masking methods were considered for fabricating an amorphous carbon thin film sensor structure and metal contacts on planar substrate. The different masking methods analysed and compared were a tape, a laser cut metal sheet and a photosensitive lacquer layer. All these were beforehand deemed suitable

for millimetre scale structures considered in this thesis.

The different methods were compared by inspecting the accuracy of the patterned structure edges and corners, especially with specific small linewidth structures. The roughness of the edges and the sharpness of the corners were visually compared, for the smoothest and the most accurate alternatives. The small structures provided additional information of the limits of specific methods as the result of the decrease in the desired width compared to the edge roughness.

The images acquired for the comparison of masking methods, were taken using Leica EC3 camera attached to Leica DM 2500 M microscope. This system was calibrated to be able to conduct length measurements from the images, which were used in calculation for deviations on the fabricated structures.

The first method, the tape used was polyester based with silicon glue with the thickness of 0.05 mm and 0.04 mm on the respective parts. Both conventional line tape and precut tape masks were examined for additional comparison. The precut was inspected for interest of better corners as the normal line tape had to be overlapped resulting in undesired effects. However, the precut tape had significantly rounder corners and wavelike edges as a result of heat present in laser cutting.

Secondly, the laser cut stainless steel sheet had thickness of 0.2 mm. Metal was also laser cut, but possessed no significant errors in the edges, yet slight roundness was inevitable in the corners. A greater issue with the metal sheet was the natural bending of the sheet as the result of thinness. This curving was further affected by the ta-C film fabricated on the surface, which possesses a significant inherent stress and thus could alter bending during fabrication. Both of these curving issues resulted in spread of the film under the mask during the fabrication. However, this behaviour was countered by forcing the sheet to bend towards the substrate surface, preventing any possible spread of the structures and resulted in more accurate structures.

Thirdly, the photo lacquer, kontakt chemie positiv 20, was applied according to the product instructions to produce a lacquer mask. For the inherent accuracy of this method the mask during which the lacquer was directed to UV-light hold high importance. These masks were either photocopies on transparencies or the stainless steel masks. The lacquer was considered as the thinnest of these mask, though the actual thickness was not determined.

3.1.3 Fabrication and structural layers

One important issue regarding the samples is the change of varying properties of differently fabricated amorphous carbon layers. Thus, the fabrication method needs to be stated in order to relate the results with other studies, at least to some extent. This subsection presents the fabrication method, and the fabricated structural layers, apart from the insulating layers already discussed.

The DIARC FCAD deposition equipment was used in fabrication of the sample structures. This is essentially, a filtered cathodic arc deposition method occurring at temperatures below 100 ℃. The sample structures fabricated consist of the actual amorphous carbon sensors, the titanium contacts and several protective amorphous carbon layers. Thus the samples are metal-semiconductor-metal structures. In

addition, two of the insulated layers were also fabricated using this method.

All the previously mentioned masking methods were studied. The majority of the structures were fabricated with the stainless steel masks as these were found to be the most suitable for the planar structures. The figure 6 illustrates several different fabricated structures used as samples for different kinds of experiments. The patters in figure 6(a) were used for measuring the resistivity of titanium contacts, yet also used in observation of the linewidth limits of fabricated structures. Structures depicted in figure 6(b) are the sensor structures used in measurements of resistance-temperature behaviour and the piezoresistive measurements. Figure 6(c) illustrates the pattern used in measuring the quality of an insulating layer.

Regarding the samples, the initial sensor structures for measuring the annealing and thermistor behaviour with four different fabrication parameters are referred with labels from S1 to S4. From these ones the most suitable parameter set was selected for the fabrication of further samples referred as K1A to K1F, which are similar to one illustrated in figure 6(b).

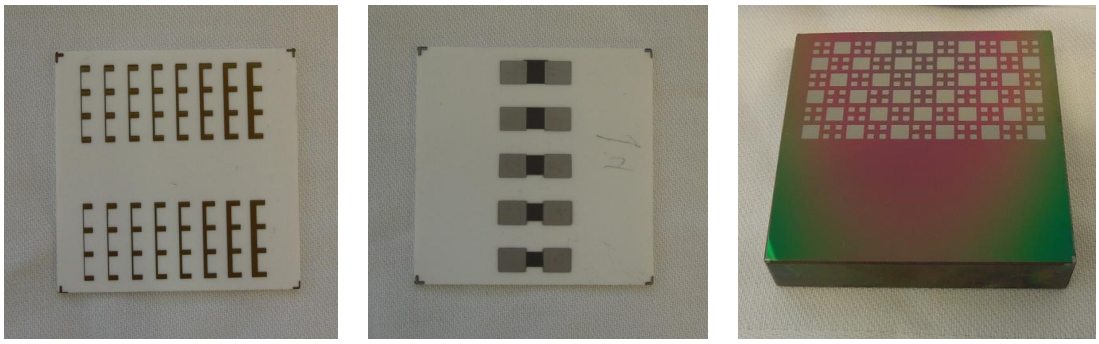

(a) (b) (c)

Figure 6: Several fabricated structures experimented in this thesis. The patterns for the four point measurements used to obtain resistance of titanium contacts (a). The sensor structure samples were fabricated on both alumina (b). The square pattern fabricated for inspecting insulating layers (c).

The layers of the sample structure on the steel substrate were the insulating layer, the a-C sensor, the titanium contacts and the protective coating layer in occasional samples. With alumina, the insulating layer was not present. The titanium contacts and the protective coating are described here, whereas the measurements regarding the sensor structure are separately described later.

Titanium, which is not an excellent conducting metal, was selected for contacts mainly because of the experience of being easily fabricated and to possess good adhesion with amorphous carbon. Additionally, titanium is known to form an ohmic contact with the sensor material, which was also examined in this study by measuring the voltage-current behaviour of several sample structures. This was done mainly for confirming the behaviour with differently fabricated amorphous carbon.

Another measurement of titanium contacts relates to the error caused by unreasonably high contact resistances, even though the amorphous carbon possesses

relatively high resistance. The resistivity of the fabricated titanium contacts was also inspected on substrates with different surface roughness. For this purpose, specific test patterns were fabricated for four point measurements on both alumina and silicon, see figure 6(a). These were examined in order to minimize the effect of the resistivity of titanium contacts on the sensor. The large resistance of the contacts would naturally decrease the weight of the sensor in the device deteriorating the sensitivity.

Additionally, several of the structures were post processed by fabricating a protective amorphous carbon coating over the sensor and titanium contacts. After fabrication of the protective coating, similar heating experiments were conducted on the structure to determine whether the protective coating causes any significant change in the structure.

The protective layer was also considered to have an effect on adhesion between layers, which is one more thing that potentially should be optimized. Several situations were inspected when fabricating the protective layer taking into account the annealing of the sensor structure. This is of interest as indicated by the previous studies on the internal stress in the ta-C structure showing decrease during annealing [23]. Thus there might be difference in adhesion between heating the structure after or before the fabrication of the protective layer.

This is related to expected problem with the metal contact, which may eventually break under the stress caused by the two surrounding highly stressed ta-C layers. The adhesion between the ta-C layers, the sensor and the protective layer, is not considered to be an issue in this respect, but anyway rather good adhesion is expected. Due to the possibility of breaking of the contacts, the protective coating was also fabricated only over the sensor structure in several samples.

3.1.4 Adhesion

The examination of the adhesion of the layers was conducted mainly by visual observation. The poor adhesion results in layer delamination or in an instant breaking of the layers when slightly touched. In cases where some level of adhesion was clearly attained, several mechanical treatments were applied to examine the level of adhesion of the samples. These tests were scrubbing with piece of fabric and ripping off with tape. Additionally, the structure could potentially be damaged by the heating or other experiments. Thus, if the structures survived without breaking during the experiments, the adhesion can be expected to be good enough.

3.2 Sensor measurements

This subsection describes measurements of electrical properties of the amorphous carbon material. Among them were the heating experiments, in which the thermistor properties were measured and the pressing and bending experiments regarding the piezoresistive behaviour.

In the resistance measurements that were conducted at room temperature, both Agilent 34970A Datalogger and Fluke Multimeter were used, with an exception of

the four point measurement of the resistivity of titanium which relied purely on the Datalogger. Otherwise, the accuracy was not expected to be diminished as the amorphous carbon material possessed rather high resistivity.

The Datalogger had resolution of 5 digits thus corresponding roughly to the accuracy of 1–10 Ω for the measured structures, and less for four point measurements of titanium. The Fluke had only resolution of 3 digits and was used mostly in situations where the accuracy was not deemed as significant. Those include measurements of the insulating surfaces and variation of the resistances between the sample structures.

3.2.1 Thermistor experiments

Several heating experiments were conducted in order to estimate the resistance-temperature behaviour of the material. In essence, two different sets of measurements were conducted to observe any permanent effect on the structure properties and the repeatability of the measured resistance-temperature curves. For both experiments, the samples fabricated with different fabrication parameters were inspected. This made it possible to obtain most suitable fabrication parameters for the thermistor, in sense of thermal sensitivity of the material.

The first heating experiment was conducted by annealing the samples and measuring the possible hysteresis and stability effects. This experiment should clarify the permanent change in the material properties. With these experiments the initial temperature limit of 600 ℃ was found too high and experiments were halted at 400 ℃, mainly due to the oxidation of titanium contacts at higher temperatures and the breaking of the sensor structure.

Another heating experiment concerned the resistance-temperature behaviour, and the respective repeatability. In this experiment, the sensor was examined based on heating, and cooling, in the temperature range of 25–200 ℃. The repeated measurements provided the information of the variation between the different measurements and also enabled a more accurate modelling of the behaviour. Before repeated heating steps, these samples were aged by annealing at 250 ℃, on the basis of the results from the first heating experiment. In addition, several samples were cycled in the vicinity of the higher temperature limit to observe delays between the material resistance change and the changing temperature.

The samples were annealed in a Nabertherm L9/C6 oven. The figure 7 shows the scheme of the actual system consisting of the sample holder and contacts within the oven. The sample is placed on top of the thermal mass stabilising the temperature of the measuring thermocouple in the middle. The titanium pads were mechanically contacted by tungsten springs, from which wiring continued out from the oven. The system was designed to be able to measure up to five structures on a single substrate at a time for gaining smaller error between the resistance-temperature behaviour of the different structures. Some issues were expected to rise due to this arrangement, mainly from the thermal mass and the location of the thermocouple.

For heating experiments the resistance was measured with Agilent 34970A Datalogger and K-type thermocouple was used for measuring the temperature. For

temperature sensing, a thermocouple is rather inaccurate device, yet more suitable for high temperatures. In any case, the thermocouple is expected to have the maximum of 1 ℃ inaccuracy in the measured range examined.

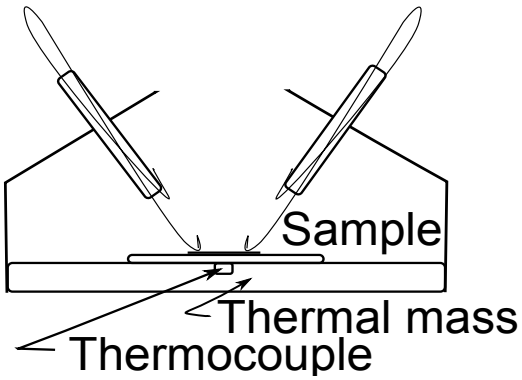

Figure 7: Heat measurement arrangement used in this thesis.

3.2.2 Piezoresistivity experiments

The main external source of the possible error of the sensor is the significant pressure present in injection molding process. Furthermore, a recent study reported piezoresistive behaviour in amorphous carbon film [27]. To observe possible piezoresistive effects, two experiments were conducted on the samples. The figure 8 presents the schemes of these two experiments. The first experiment (8 (a)) was carried out by pressing the part of the sensor structure with a known force and roughly known contact area and measuring any changes on resistivity. The force is used in defining the pressure on the surface, as on the rougher surfaces the contact area might differ from the actual surface area pressed.

Another experiment was the test of bending of the substrate, which causes shear stress for the thin film structure. The behaviour is expected to be different when the substrate is bent in different directions. The direction of bending is defined with the surface with the fabricated film. As in the figure (8 (b)) the bending would result in concave surface of the film. The opposite case, where the sample is turned, is the convex case. These both cases were inspected as the internal stress of the amorphous carbon film might have an effect on the piezoresistive response.

In case of pressing and bending experiments, the sample was respectively lying on the level surface or attached from the other side. Force for pressing the sensor or bending the whole substrate was directed with a shaft with a vertical roller having the weight of 300 g. Additionally, several weights of roughly 1000 g and one weight of 500 g were used in the measurements. The resistance was measured using the Datalogger wired to the titanium pads with silver adhesive. In case of pressing experiment, a tape was attached onto the tip of the shaft and cut to a rectangular shape with an area of around 20 mm^2, thus relating one newton force into roughly fifty thousand pascal pressure. In bending, the substrate was bent by pressing the edge opposite to the attachment.

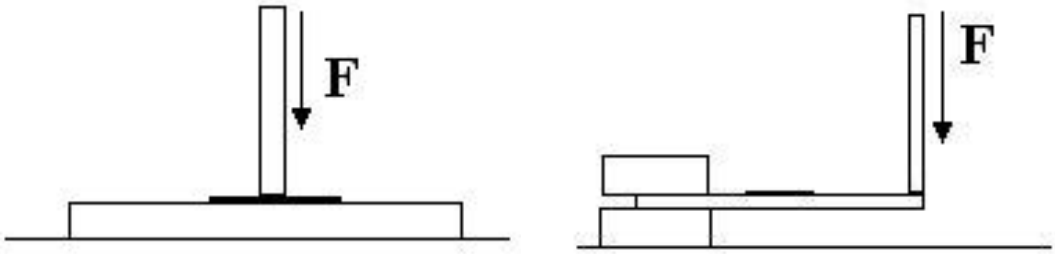

(a) (b)

Figure 8: The schemes of measurement arrangements used to determine piezoresistive behaviour.

For other errors related to piezoresistivity, the microphonic behaviour was examined. This is of interest as mechanical vibration is present in industrial application. These vibrations can prove actually to be a significant source of error, assuming that the material possesses microphonical properties.

The microphonic behaviour was measured attaching a sample sensor on the structure of a machine, which was known to produce mechanical vibrations at a reasonably constant frequency of around 10 Hz. The effect of this vibration on the sensor resistance was then measured using the Datalogger. To observe the effect of wiring on the resistance, a commercial resistor was measured and compared simultaneously with the sensor structure on alumina. As the conventional resistors are manufactured to minimize external errors this allows deduction whether the microphonic phenomenon occurs.

In the measurement, the Datalogger sampling frequency for high resistances was roughly 7 Hz with the two structures simultaneously measured. This causes inaccuracy in the measurements, as five measurements are required to obtain sufficient information from a single period. The comparison with the resistor is still possible for the detection of the microphonic behaviour.

4 Results and Discussion

The conclusions made from the executed experiments indicate that the fabricated amorphous carbon film functions as a thermistor. Furthermore, after ageing the material through annealing, this property was found to be repeatable rather accurately following the hopping conductivity model. The problems regarding the heating arrangement are discussed and shown to have only a minor effect on the obtained results. The material is also found to possess piezoresistive behaviour that is negligible compared to changes associated with changing temperature.

Regarding the device fabrication, these properties were observed both on alumina and steel substrates. The fabrication of the film on the steel substrate required additional process before deposition, which resulted in a varying effect on the resistive properties in form of metal layer beneath the fabricated film. This issue was associated with the insulating layer and also caused further difficulties with protective layer. The amorphous carbon protective layer itself was found as a plausible wear-resistant layer.

This section is organized as follows. The first part of this section presents a separate analysis of the masking methods, followed by the results for the main part, a ta-C thermistor sensor structure. The section is finished by the discussion of other experiments conducted.

In the main part, the actual thermistor behaviour is discussed first, covering essentially the resistance-temperature behaviour of the material. This part contains observations regarding annealing and the resistance-temperature behaviour. These observations are used in the modelling of the sensor behaviour and estimating the accuracy of the thermistor and variation in the fabricated structures. The heating arrangement issues are also considered in order to enable drawing correct conclusions from the obtained data.

The other experiments were made in order to check if there are other factors affecting the sensor resistance or properties important to the overall structure. The things concerned were those related to the application of the sensor, an injection molding tool. Thus, the effect of the pressure on the resistivity of the sensor is crucial. Additionally, the structure resistance is examined for the presence of microphonic behaviour, which essentially is the effect of the mechanical vibration on the structure.

Secondly, the titanium contacts were studied for their conductivity on the selected substrates. Another experiment regarding titanium was the inspection of the current-voltage curve of the fabricated sample structures to confirm the ohmic contact over the metal-semiconductor junction. The insulating layers on the steel substrate are also compared in terms of their insulating properties. The most important property being the number of cavities on the layer possibly contacting any fabricated films to the substrate. These results can be used for optimizing the width of the titanium contacts, minimizing both the possibility of contacting the steel substrate and the effect of the resistance of the contacts on the whole sensor structure.

Finally, there is discussion regarding any adhesion problems observed between

the fabricated layers and the protective coating. The effect of the protective coating is also examined with respect to other results.

4.1 Masking analysis

This section discusses the differences and suitability of different masking methods on the substrates used. The differences with different methods, tape, lacquer and steel stencil masking, were not significant in regard of the accuracy of the patterned structures required. Nevertheless, the steel stencil was found to be as the most suitable alternative due to the lack of chemicals and resulting problems with adhesion.

The differencies in the masking techniques are mainly considered through differences in the accuracy of the fabricated structures with respect to the masking pattern. The factors considered are the edges and corners of these structures, but also the fabrication of small structures and variation of desired line widths were examined. The accuracy of the fabricated structures is not likely to differ greatly with different substrates, but the adhesion of the fabricated structures might differ. In this aspect, the different substrates are masked with different techniques and the adhesion of the layers is examined by mechanical treatment and by heating of the fabricated structures.

Figure 9 illustrates the accuracy and quality of different methods showing the corners of fabricated structures. The tape and lacquer masked structures show deteriorating of the edges of several dozen microns. Though the stencil masked structure possesses much cleaner edges, there is limited spread of the fabricated layer outside the patterned structure.

These observed anomalies are related to several issues, where inaccuracies are caused by different masks. The steel substrate, in which edges were the least rough, required additional structure to force the sheet firmly on the surface. Otherwise, the fabricated material would have spread too much. The spread does not significantly affect the resistance of the structure, being thinner and poorer in quality. The poor adhesion of the layer may cause the spread, or structures being fabricated over the spreading area break off.

Tape and lacquer were sufficiently similar in accuracy, the accuracy of the latter was mainly diminished by the issues with applying lacquer and the development of patterns. The former had problems with adhesive, especially on the corners of the structures. The corners were patterned with overlapping tapes that resulted in the poor quality of these parts in the fabricated thin films. Laser cut tape on the other hand had rather round corners and wave like edges due to heat present in the patterning method. The resulting accuracy of both lacquer and tape maskings were decent and comparable with the steel masks. However, the fabricated pattern edges contained a narrow zone with slight cracking and other deteriorated structures, which can be significant especially for smaller structures.

Another property compared between different masking methods was the effect on adhesion in various coatings. The coating initially covered well the area designated by the mask, by the use of all chosen methods and substrates. However, as in figure 9, the film broke off on the structure edges when the lacquer was removed and simi-

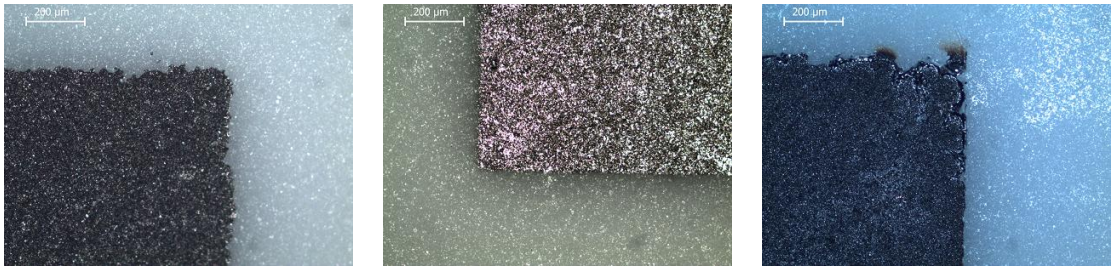

(a) lacquer (b) steel stencile (c) tape

Figure 9: The corners of the structures fabricated with different masking methods.

larly when tape masked samples were cleaned for following fabrication phases. This supposedly associates with the residual chemicals from tape glue and the lacquer on the patterned area and from the flow of the same substances in vacuum on the masking border.

As assumed, there were no significant differences in the accuracy of using different substrates. The smoother substrate resulted in somewhat increased deteriorating in the layer edges with lacquer and tape masks. The increased deteriorating is likely caused by the easier flow of the substances on smoother substrates in vacuum. The chemicals are not trapped within the bores of the rough alumina layer, but instead lay on the smooth silicon surface.

In addition, in the case of the lacquer and the alumina substrate the rough surfaceled to a situation that the photo sensitive lacquer remained partially on the patterned area after developing. This resulted in poor adhesion of ta-C and titanium structures that tended to break at temperature of roughly 200 ℃. For other methods no major problem was found at such temperature. Yet, at the same temperature a minor increase in breaking of the edges of the tape masked structures was observed, in addition to deteriorating at room temperature. This is caused by trapped particles on the substrate, which are not affected by post cleaning of the sample or lacquer removal, but vaporizing and breaking the structure when annealed. The metal masks did not bring along such problems with adhesion, as no additional chemicals were used for attachment. However, the nature of fabricated structure caused the ta-C film to flake off at the edges when annealed to 350–400 ℃ .

4.2 Thermistor properties

This section contains the main results of this thesis. The section describes the behaviour of the fabricated sensor as a thermistor on the basis of the heating experiments. Both substrates, alumina and insulated steel, are considered, though the majority of the experiments and the discussion concerns the alumina samples and the use of the steel substrate is merely compared with alumina. Also, differently fabricated samples are examined to find the most suitable candidate in terms of fabrication parameters.

The first part discusses the effect of annealing and the permanent changes from

the room temperature resistance. The second part concerns the issues of the heating arrangement, which is addressed in order to justify the results and to give a correct interpretation. The results are analysed in order to obtain the resistance-temperature behaviour of the materials. Based on the observed behaviour, the suitable model is obtained from the available candidate ones. Finally, there is discussion related to the variation of the fabricated structures, due to masking and fabrication parameters.

4.2.1 Annealing

The annealing of the material was found to permanently decrease the room temperature resistance of the film through structural changes on the material. However, these changes are stabilised after a sufficient annealing period, which makes the behaviour a viable ageing method to prepare the film for thermistor purposes.

The inspection of the thermistor properties of amorphous carbon is started by observing any changes on the material during annealing. The inspection is conducted on a set of four differently fabricated samples with the same dimensions on alumina substrate in order to find the best candidate for the fabrication parameters. For convenience these samples are referred to as S1, S2, S3 and S4. The difference in the fabrication parameters of these ta-C structures cause a significant change in the resistivity of the structure.

According to the presented theory, the difference in the resistance is associated with the microscopical structure of the fabricated film, which depends on the fabrication parameters. The change of parameters used in fabrication most likely resulted in changes of sp^2 fraction of the material. This would increase the localised states in the mobility gap that would further increase conductivity due to hopping through these states. Furthermore, the similarity of the resistances measured from the last two samples indicates the saturation of the formed structure, as no effect was seen with further change in the fabrication parameters.

The annealing of ta-C results in a significant irreversible drop in resistance. The figure 10 describes the proportional change of the room temperature resistance as the function of the annealing temperature, up to 400 ℃, for different fabrication parameters. This clearly shows that the proportional change in resistance due to annealing notably differs between the samples. This is related to the relaxation of the network [22, 23]. The annealing causes relaxation of the ta-C network reducing the resistance in the system due to reorganization and the creation of sp^2 sites.

However, the annealing process cannot be described merely by the maximum temperature. The structure is still undergoing a change at the reached temperature when the annealing is halted and the sample starts cooling. Thus the structural change, due to annealing, does not solely correspond to a specific temperature, but to the annealing time as well. This results in the specific amount of structural change in the material. The structures were aged by annealing and keeping the temperature until the resistance decrease was sufficiently slowed down, which corresponded to roughly a time of one hour and was slightly longer at higher temperatures. Thus there is some variation in the achieved level of resistance as the amount of structural

change cannot be explicitly determined.

The repeatability of the sensor structure was deemed nonexistent due to the permanent change in the resistance when annealed. On the other hand, the figure 11 with successive annealing curves, suggests that when the material is annealed to the same temperature for a second time, the structure reaches the same resistance. The resistance tends to decrease very slowly to the stable value, which causes continued change in resistance with consecutive annealing to the same maximal temperature.

These observations give a natural approach to solve the issue and further study the repeatability and amorphous carbon as a potential thermistor material. The annealing can be used to age the structure at a higher temperature than the temperature of intended use. This method would also enable the actual measurements of the resistance-temperature behaviour and also modelling this behaviour. Additionally, it must be noted that the structure was damaged, yet still working, when annealed at temperatures between 350 and 400 ℃. This would establish the upper temperature limit for annealing and operation.

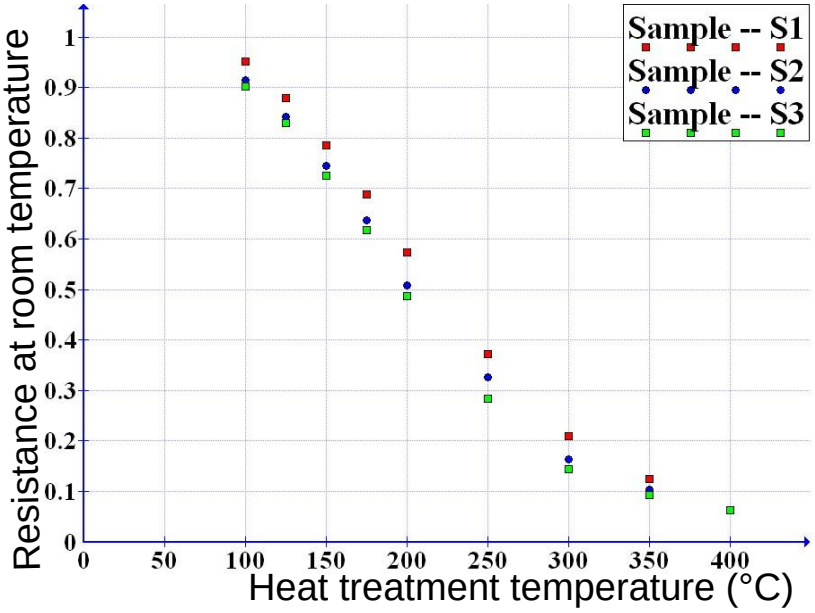

Figure 10: The proportional resistance change at room temperature, when annealed to a specified temperature.

The behaviour during annealing differs significantly for some samples on the insulated steel substrate, due to the different fabrication parameters needed to obtain the necessary adhesion of the sensor. The layer composed of aluminium and magnesium oxides was used as the insulation on the steel substrate. There is a noticeable step on the annealing curve of the sample as seen in figure 12, in comparison to the annealing of alumina shown in figure 11. Additionally, the room temperature resistance of the steel samples is increased as a result of annealing. Also, the initial resistance of the samples where this step was observed was considerably lower compared to other samples, regardless of the corresponding dimensions, even though they originated from the same fabrication batch.

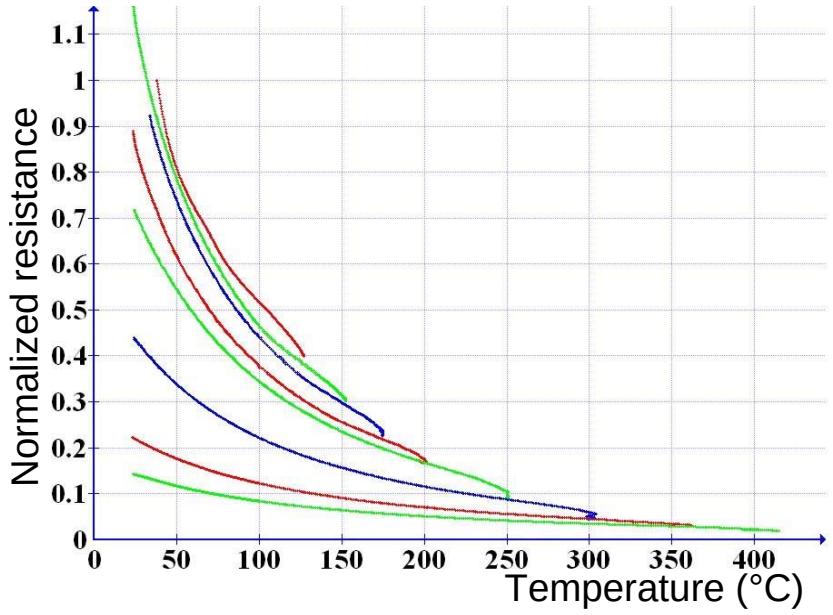

Figure 11: Successive curves for annealing a sample up to 400 ℃ . It is clearly seen that when annealing is halted the following heating reaches the same resistance near the maximum temperature of the treatment. Also the ends of annealing curves display decrease in resistance as the given temperature is maintained.

A reasonable explanation for this behaviour could be a metallic layer beneath the sensor structure, which effectively lowers the resistance. The step in the temperature-resistance curve after 100 ℃ corresponds to the temperature in which this metal reacts and raises the resistance of the metal layer, through oxidation or other processes. The specific insulating layer is composed of aluminium and magnesium oxides of which the latter easily forms compounds both with oxygen and nitrogen at relatively low temperatures. This process is reasonable as in later measurements with an annealed sample the step is no longer observed, see figure 16.

However, after annealing the sample did not show a similar behaviour as those samples on alumina, but rather a more linear dependency between resistance and temperature(see section 4.2.3 Resistance-temperature behaviour). This linearity would result from a fortunate combination of the exponential resistance-temperature behaviours of the assumed metal layer and the amorphous carbon film. Anyway, nothing absolutely certain can be said of the separate resistance contributions of the layers without better information of the layer beneath the sensor. In contrast, the other samples of the batch did not present the clear indication of the disturbing layer in the form of altered annealing curve or in the behaviour seen in the successive heating experiments. However, their ratio of room temperature resistance after and before annealing to 250 ℃ was observed to be only roughly 50 % instead of 37 % observed with alumina substrate. This certainly indicates that the layer is present and must be taken into account in the device fabrication.

These observations mean that the disturbing layer can have a varying effect on the whole structure. The layer can be so thin or damaged that it leads to

resistance that is orders of magnitude higher than that of the sensor, resulting in the similar behaviour observed on alumina. In any case, the fabrication process needed to achieve sufficient adhesion of the amorphous carbon film poses difficulties for manufacturing the structures, as a single batch produces two kinds of sensors, those with and those without the disturbing metal layer.

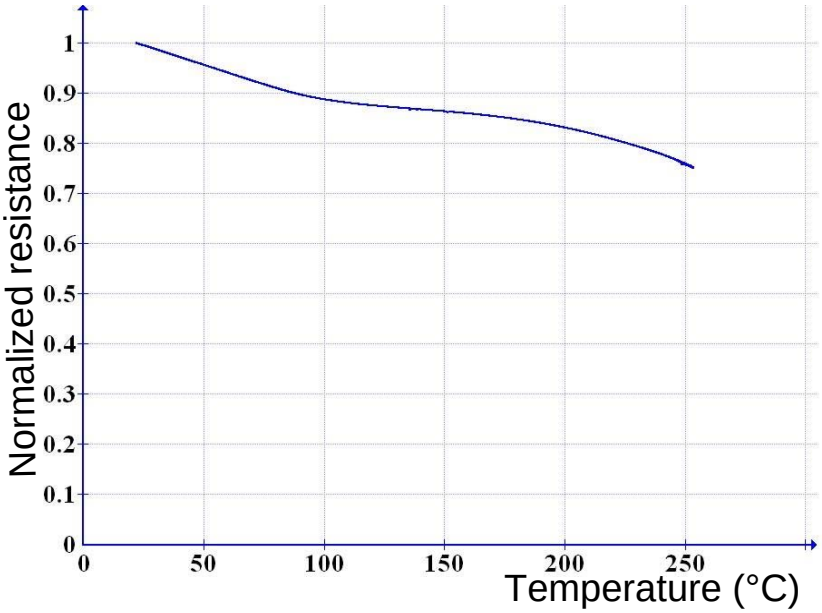

Figure 12: Resistance-temperature curve of the sample on steel substrate when annealed to 250 ℃ for ageing.

4.2.2 Heating arrangement

The concerns related to the heating arrangement need to be addressed before the discussion of resistance-temperature behaviour. There are several issues with the heating arrangement, which may affect the interpretation of the results and alter the resistance-temperature curves observed from the actual behaviour. In initial annealing, the arrangement does not cause any problems. The variation of the heat treatment time makes the inaccuracy that is caused by the heating arrangement irrelevant. For analysing the repeatability of the resistance-temperature behaviour any inaccuracies caused by arrangement need to be discussed. This section shows that the arrangement used in this work is suitable, yet crude, for measuring thermistor behaviour of the fabricated thin films.

The main concern in the arrangement is that, though the oven is well insulated, air inside is still cooler than the surfaces with the heat elements. Thus the sample may either be placed on the heat element or separated by air. The former would cause significant dependency of the presence and the activity of the heat element, which causes difficulties in placing the thermocouple. The latter results in the difficulty in the temperature measurement since any sensor would be placed in air, of which temperature varies with position inside the oven. This variation causes a

problem, when the thermocouple used to measure temperature is in air with the sample. The heat capacity of the thermocouple is insignificant compared to the sample with a bulky substrate, which results in significant difference in actual and measured temperatures. Even though the sensor is a thin film on the surface of the substrate, this difference affects the measurement. Placing the thermocouple between the sample and heating element, would not solve the issue with large difference between the heat capacities.

To solve this issue, a thermal mass, a body with a large heat capacity, was introduced in contact with the sample and thermocouple. The presence of the thermal mass would decrease the effects from the fast changes in temperature and the differences in temperature distribution within an oven. With both the thermocouple and the substrate affected by the thermal mass the thermocouple will correspond better to the slower heating of the sample.

However, this does not eliminate the possible difference in the temperature measured by a thermocouple and the actual temperature of the sample. The carbon thin film structure is located on top of the sample in the interface between the substrate and air. Thus the film temperature is essentially that of the surface, which lies in between air and thermal mass. The temperature difference results in clearly separate parts of the heating process. First there exists a clear beginning and end of heating, where the measured temperature and air temperature in the oven begin to deviate. In the middle there is steadier part where the heating is steady and also the difference between measured and actual temperatures is sufficiently constant.

The arrangement is justified by assuming that with experimented temperatures the difference between air and the thermal mass temperatures does not vary significantly. Significant variation would cause bending of the resistance-temperature curve, which in turn would result in possibly false interpretation of the model. Some changes are nevertheless expected, especially with the beginning and the end of the heating or cooling processes.

The temperature of the thin carbon sensor is mainly expected to deviate from the measured temperature as air has considerable effect on the surface temperature. Regarding the sample substrates, both alumina and steel possess similar heat conductivities, which being reasonably large cause only a minor delay in the heat transfer through the substrate. This delay should result in actual temperature of the sensor being typically higher during heating and lower during cooling than the measured temperature.

This behaviour was examined by adding another thermocouple measuring the surface of the sample K1E. Though it is difficult to conclude to what extent this thermocouple measures the temperature of the sensor film or even the surface, some insight is nevertheless gained from the behaviour with the two thermocouples. Figure 13 illustrates the extremal points of the measurement of both thermocouples and of the scaled resistance with respect to time. The measured temperature of this sensor corresponds significantly better to the resistance curve measured when compared to the probe attached on top of the sample. This justifies the use of the thermocouple between the thermal mass and the sample. However, the expected difference in the actual and measured temperature cannot be confirmed with this experiment. The

separation of the surface temperature and measured temperature is expected to be less than that deduced from the figure, which is 2.4 ℃.

Another measurement was also conducted in which the temperature in the oven was raised in steps, letting the system stabilize. This resulted in resistances that corresponded well to the cooling curve obtained with the thermocouple below the sample. Thus, a more accurate analysis should use data associated with cooling, where the temperature differences in the oven are lower during the process.

The steel substrate is affected in a similar manner. The thick substrate thermally separates the sensor structure and the thermocouple. Thus, the sensor is expected to heat and cool faster than the measured temperature, more noticeably than the alumina sample.

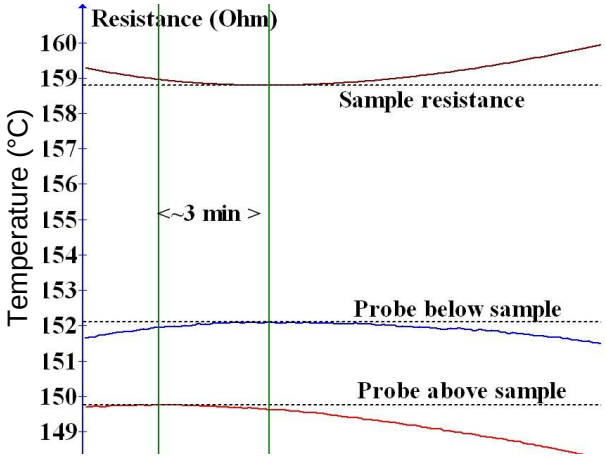

Figure 13: Measured temperatures of the probes below and above the sample compared with the resistance measured with respect to time. Clearly the probe below corresponds better to the resistance measurement during the change between heating and cooling.

The assumptions for the behaviour of the measurements are proven in figure 14, which illustrates the measurement of resistance and temperature as a function of time when heating to 200 ℃. The resistance is scaled for easier comparison. These curves show that as the thinner alumina sample, K1E, shows no observable difference in the switch points of resistance and temperature. This means that there is no major delay in heat transfer through the substrate, though there can be difference in the measured and actual temperatures. For both substrates, this makes a difference as the temperature limit is reached for the first time, which might be caused by the speed of heating.

For a steel substrate this first switching is the only point at which the turning points of measured temperature and resistance correspond well with time. Similarly, a more noticeable, behaviour is observed in all subsequent switches, as the extremal values of resistance and temperature deviate more with time. This is likely to be related to the thicker substrate, which causes delay in the thermal transfer. During switch between the heating and cooling, the transfer occurs through the thermal mass to the substrate during switches, explaining the deviation in extreme values.

This is acceptable as the oven reached the temperature of 200 ℃, yet the thermal elements are actually at higher temperature, resulting in the difference of opposite kind.

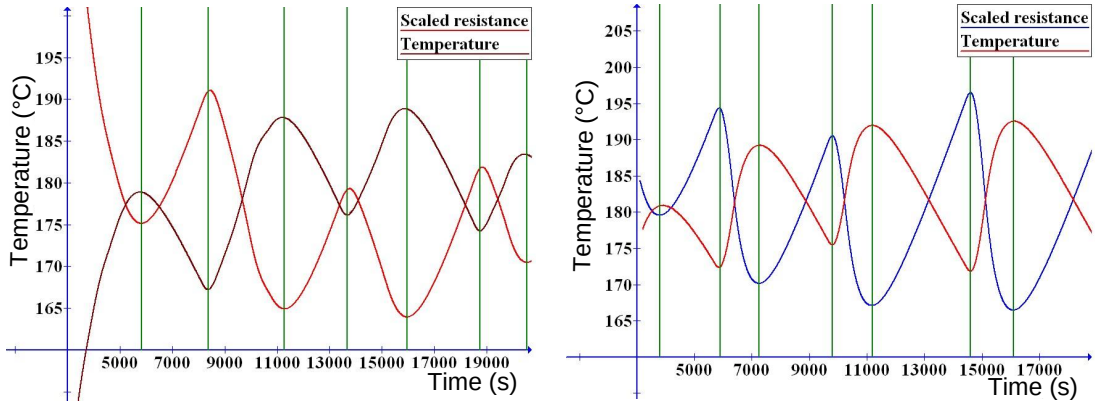

(a) Steel substrate (b) Alumina substrate

Figure 14: The comparison of the resistance and temperature with the time of measurements for different substrates during subsequent cycles of heating and cooling. The resistances are scaled to enable time dependent comparison. These indicate the assumed behaviour for different substrates. Vertical lines are added to help to locate the differences between the extreme values.

These difficulties complicate the interpretation of hysteresis and other phenomena occurring during switching between heating and cooling. The latter phenomena cause no major problem as the relation between temperature and resistance can be obtained during steady heating or, preferably, cooling process. This behaviour should neither cause significant difference in the actual behaviour and associated real hysteresis, assuming that the temperature is allowed to stabilize and the temporal deviation is not present, as in case of alumina. The error due to hysteresis can also be evaluated between steady states in a process between heating and cooling. However, this gives a crude estimate as the air temperature during cooling and heating is higher or lower than the measured temperature, respectively. This causes possibly larger separation of the curves, distorting observations of hysteresis.

4.2.3 Resistance-temperature behaviour

This part concerns the resistance-temperature behaviour and the respective repeatability. The exponential dependency between temperature and resistance is observed and found to possess good repeatability on the aged samples. The hysteresis of resistance is found negligible compared to the measurement inaccuracies, being less than 0.25 ℃.

Both the repeatability and the resistance-temperature behaviour after annealing at a higher temperature were studied using alumina substrate with a set of four differently fabricated samples (S1-S4), from the same batch as the annealing samples.

Each sample contained two test structures, A and B, which were inspected simultaneously. These were initially annealed at 250 ℃ and afterwards repeatedly heated to 200 ℃. Figure 15 shows average temperature behaviour normalized at 50 ℃of the A structures. This shows the resistance sensitivities of different samples that indicate the fabrication parameters of S1 sample structure being the most sensitive. All the curves follow some exponential behaviour though the actual form shall be discussed later together with the model. This already proofs that amorphous carbon material acts as a thermistor.

The figure 16 illustrates the behaviour of samples on a steel substrate, which differs in varying degree due to metal layer beneath the sensor. With smaller effect from the disturbing layer the resistance has dropped to roughly one quarter of the initial at the temperature of 200 ℃. Which is slightly larger than similar drop for samples on alumina between normalization point of 50 ℃ and the upper limit of temperature range.

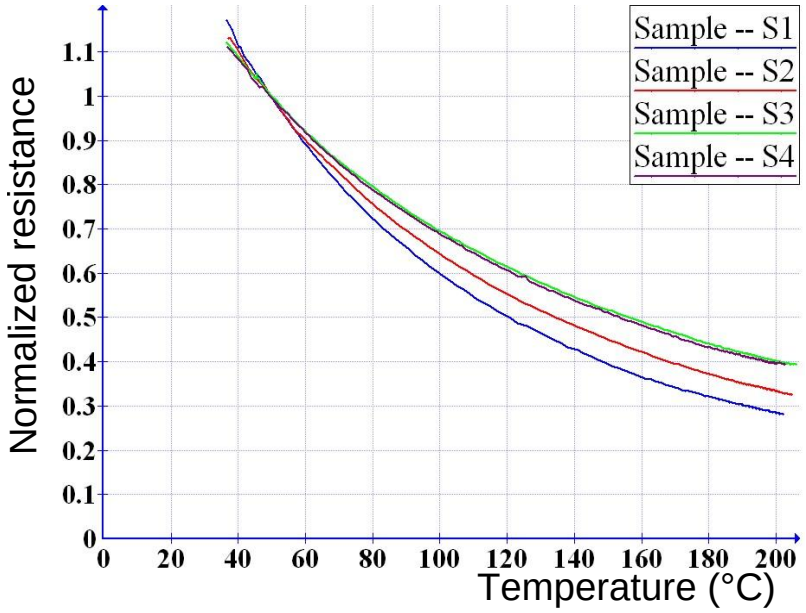

Figure 15: The average temperature-resistance curves of the different samples normalized at 50 ℃.

The repeatable behaviour is observed in consequent heating curves, yet during cycling the material can still exhibit hysteresis. The figure 17(a) presents cycles around 180 ℃ measured for a sample on a steel substrate. This data corresponds to the figure 14(a) describing the time behaviour of the measurements, thus meaning that the observed cycles are actually caused by delay in the measurements. When compensating this delay by matching the extremal points of measurements, the samples show a similar behaviour as on alumina substrate shown in figure 17(b). Thus, the hysteresis can be expected to be roughly 0.1 ℃. The measured resistance can also have a separation of roughly 0.1 % from a value at a specific temperature.

For the more evident results of the low level of hysteresis the alumina expresses similar results without a need to compensate the delay, as a result of a much thinner

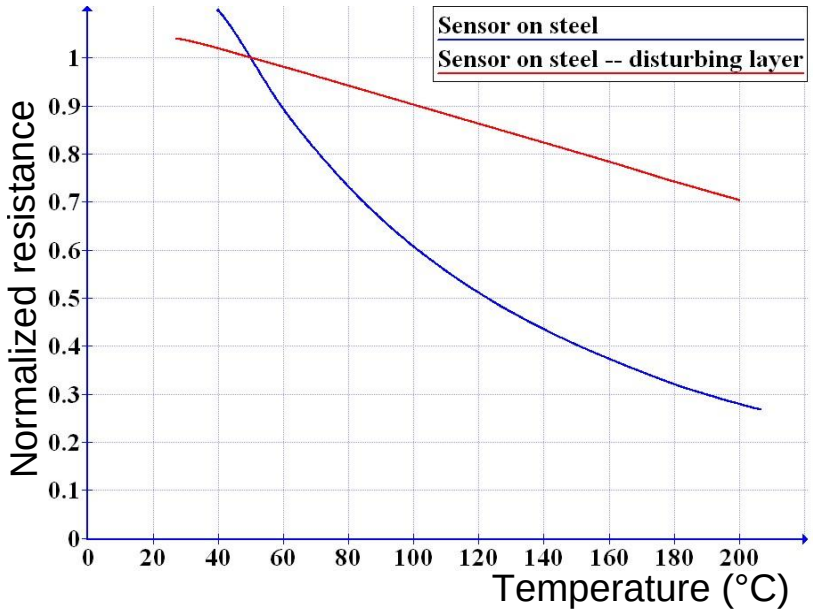

Figure 16: The temperature-resistance behaviour of annealed sensor on steel substrate, with and without the disturbing layer.

sample substrate. For alumina, the result of a similar measurement is illustrated in figure 17(b). The figure indicates that the hysteresis is less than a quarter of a degree or roughly 0.1 % of the resistance. Similarly as for the compensated results on the steel substrate samples, this shows suggested behaviour due to thermocouple placement, though the final level of temperature is roughly reached only after several cycles. At the first switching point the measured temperature is roughly 2.5 ℃ less than the actual temperature, which results from the fast pace in the heating process and the large thermal mass.

The hysteresis measurements additionally confirm the assumption that ageing at higher temperature effectively stabilised the structure at slightly lower temperatures. The cycles in figure 17 do not exhibit any behaviour indicating the decrease of resistance and thus no permanent structural change in the material.

4.2.4 Accuracy

The behaviour of the thermistor has been established and was observed to be repeatable. Further examination of the measurements determine the accuracy between the measured resistance and temperature. The effect of hysteresis is already considered and found minimal, this section shows that the variation between the measurements with the same sensor is less than half a degree or 0.4 % of resistance near the temperature of 200 ℃.

The repeatability of resistance-temperature curves was inspected with additional samples containing five structures each with fixed length and varying width referred as K1A to K1F. The data for estimating the repeatability between the heatings of a single structure consists of two different experiments with the sample K1B and K1E.

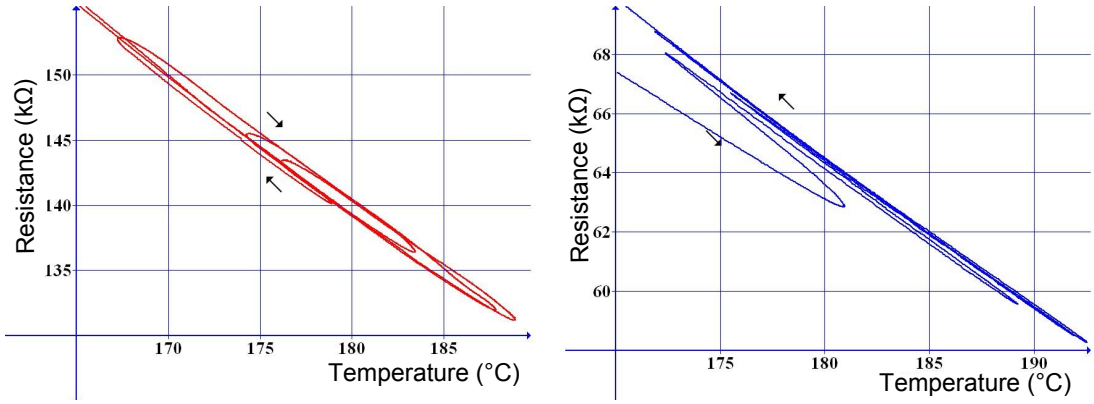

(a) Steel substrate (b) Alumina substrate

Figure 17: The cycling of temperature and the corresponding resistance for a sample on a steel substrate (a) and an alumina substrate (b). The arrows indicate the direction of time in measurements, the heating occurs on upper curves for steel and lower curves for alumina and opposite for cooling. This shows the suggested behaviour of actual and measured temperature and gives crude error due to hysteresis.

The data obtained from the other samples was used in computing the variation in respect to the repeated measurements on the fabricated structures. First, the six heating curves of the sample K1B are measured between the room temperature and the temperature of 200 ℃ after annealing at the temperature of 250 ℃. Secondly, three cooling curves of K1E from 180 ℃ to roughly 100 ℃ are considered in drawing more accurate conclusions. As noted, the heating possesses slight inaccuracies, yet the data gathered is obtained through similarly conducted heating procedures and thus causes no error when concerning the error in the repeatability.

The combined data of measurements is averaged with respect to both temperature and resistance. The combination is done as the data consist of time spaced values for both temperature and resistance, thus corresponding values are not obtained for each measurement. The pooling of the data from measurements was deemed suitable, as the number of measurements pooled were tightly spaced in temperature scale. Thus, the tightness of pooled measurements caused no major increase in the error. As a fixed amount of values is pooled, the error in stable heating period is larger compared to the slower phases at the end and beginning of heating.

These two different measurements are expected to have a significant difference in the error of a single structure, caused by different speeds of heating and cooling. The nature of the experimental arrangement suggests that the variation in the initial temperature of heating can displace the curve between subsequent heating experiments. This results from the fact that the initial temperature varies by a few degrees and the oven reaches some stable behaviour after which temperature rises sufficiently linearly.

In cooling there also is expected to be some variation with the initial point of cooling as temperature can only be determined with an accuracy of a few degrees. However, the cooling process itself is slower and more stable since there is a smaller

deviation in actual temperature, air temperature and thermocouple temperature. The differences in two measured points are roughly half a degree for heating and less than tenth of a degree for cooling, thus the difference in pacing and accuracy is imminent. Additionally as seen in the figure 17(b), the stable temperature would be reached only after several cycles, when measuring with alumina substrate. This means that the heating curve does not represent the actual behaviour between temperature and resistance in the latter part of heating. In terms of the error between measurements this does not cause significant problem as the measurements are performed similarly, excluding the variation of the initial state.

The proportional error for the first experiment is presented in figure 18(a) as the standard deviation between different measurements. The initial part of the error curve indicates variation in the heating process and starting temperature. This stabilises to roughly 0.6 % when temperature difference between thermocouple and the sample has become sufficiently constant, which occurs after 80 ℃. Around 180 ℃ the error drops as heat transfer slows down when air temperature of the oven has reached the preset value. The air temperature is then kept constant in the oven, which causes measured temperature to increase in lower pace. Thus measurements are more dense in temperature and the deviation decreases towards 0.3 %.

The proportional error of the second experiment is illustrated in figure 18(b). As is the case with heating curves, the higher error near the starting temperature of 180 ℃ results from the initial variation and decelerating cooling. The cooling begins to slow down after roughly 170 ℃ due to the difference between air and thermal mass temperatures reaching its maximum value. There is no similar steady process as in the case of heating as air quickly cools down and then the whole system steadily cools down. The increasing error with temperature is associated directly to decreasing resistance of the sensor, increasing the proportional effect of the initial deviation in resistance. With this measurement, the standard deviation of the resistance is below 0.2 % during cooling on the measured temperature range.

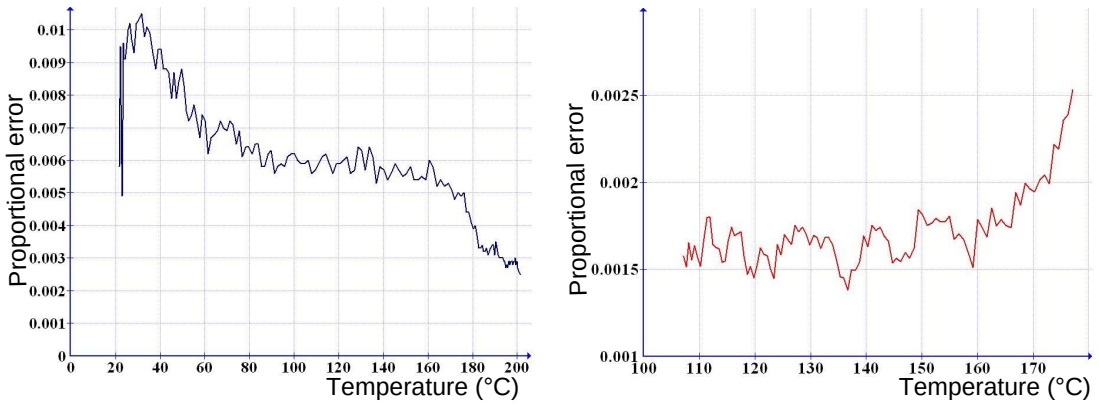

(a) Heating (b) Cooling

Figure 18: The proportional error in the measurements of resistance-temperature relationship given as the standard deviation, for heating (a) and cooling (b) measurements.

Finally, when considering the error in presented measurements of the sensor, the deviation in temperature must be computed. This depends on the variation in measurement, error due to hysteresis or due to external forces altering resistance cause deviation. The hysteresis was already found to cause up to one quarter of a degree deviation in temperature calculated through the sensor resistance. Several external error sources are discussed later. Other sources have to be related to the rate of change of resistances with respect to temperature. When one can tell what proportional change in resistance is caused by one degree change in temperature, the error can be approximated. For this purpose the temperature coefficient of resistance

$$\alpha_T = \frac{1}{R(T)} \frac{dR(T)}{dT} \tag{3}$$

is obtained from the measured data. The coefficient data is plotted for two heating experiments with alumina, K1E, and steel substrate samples in figure 19 with respect to temperature. The figure shows that the coefficient is around 0.012 for the resistance though it tends to decrease with increasing temperature in case of aluminium oxide sample aged by annealing to 250 ℃ . The similarly treated steel sample follows a similar curve as the alumina sample, though the structure on steel seems to have weaker sensitivity to temperature. However, the different behaviour is explained by the role of the metal layer below the sensor structure.

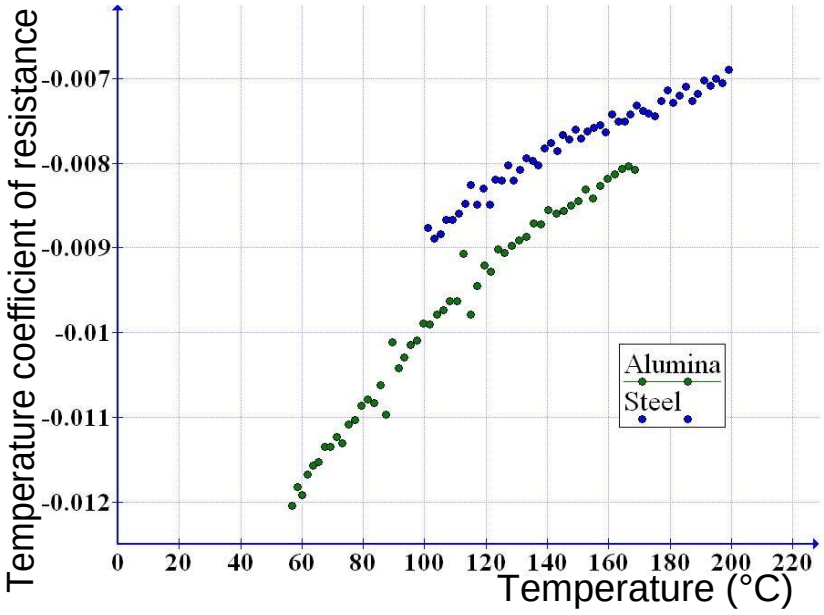

Figure 19: The temperature coefficient of resistance of two heating measurements as a function of temperature.

Presented data relates the variation of resistance to the variation of measured temperature. The error in the resistance measurement at a specific temperature corresponds to a range determined by the change of resistance with temperature. The resistance was computed to have proportional standard deviation of 0.2 % between measurements during a stable phase. The measured temperature differs,

in terms of standard deviation, from actual temperature by less than 0.5 ℃near the temperature of 200 ℃.

4.2.5 Model

As the structure was shown to contain a thermistor and also otherwise act like a rather standard semiconductor, it was expected that exponential resistance-temperature behaviour is an exponential function. This behaviour is found to follow hopping conductivity model in the whole measured temperature range, from room temperature to 520 ℃.

The issues with the heating arrangement have to be taken into consideration when fitting either extended states or hopping conductivity model. Thus, one must still note the existence of the different temperatures of the oven, the thermal mass and the sample. Air in the oven cools and heats faster than either the thermal mass or the sample. Thus it is expected to slightly alter the curvature of the fitting caused by the varying temperature difference between the different elements in the oven. These cause opposite changes in the behaviour between heating and cooling processes because of the opposite temperature differences. This slight deviation causes only minor error during steady heating and cooling phases, where the temperature difference is sufficiently constant. More disturbing behaviour is seen in both the beginning and the end of treatment, where the temperature differences quickly alter, causing significant bending of the curve.

Other two issues that have been already noted, the heating that needs stabilization in the end and the temporal error in the measurements with the steel substrates, also contribute to the shape of the curve. The former causes increase in curve steepness affecting the exponential parameter. The latter is not a major concern during the steady process, though would result in altered multiplier in both models.

Though these are likely to affect the parameters of the model, the behaviour in conduction is expected to clearly follow either of the models. This statement is motivated by the opposite effects during heating and cooling, thus real behaviour is seen by observing these two measurements. Thus the conduction behaviour shall be established first and variation in model parameters is concerned later.

To determine the method of conduction, the logarithmic resistance is plotted against inverse temperature. The plotted curve should be linear, if the conduction occurs through the extended states, following model in equation (1). The figure 20(a) shows a nonlinear behaviour measured from a structure on steel substrate heated to 470 K. To show that the model of variable range hopping, depicted by equation (2), is more suitable for describing the behaviour, the figure 20(b) has the same data against the fourth root of inverse temperature. The straight line shows that the data is much better fit using variable range hopping model.

Interestingly, there is no sign of the activation of conduction between the extended states in measured temperature ranges. Furthermore, a sample, K1B, on alumina substrate was annealed to 570 K and the temperature-resistance behaviour was afterwards examined up to 520 K. In this case, there were neither observable switch in the behaviour as seen in figure 21. Thus the specific amorphous carbon

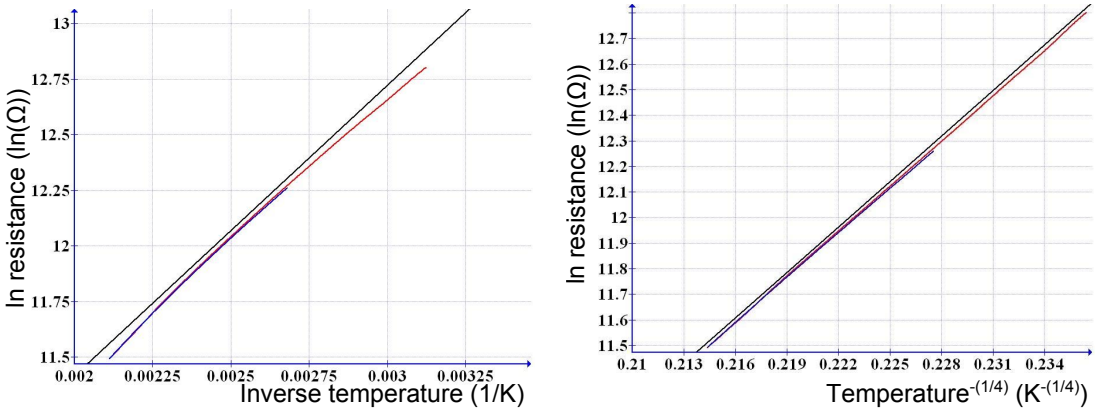

(a) (b)

Figure 20: The natural logarithm of resistance versus the inverse of temperature (a) and the fourth root of inverse temperature (b). The linear dependency and minimal difference between the heating and cooling curves suggest that conduction occurs through hopping. Straight black lines are added as a guide to the eye.

studied in this thesis possesses hopping conductivity as a major conduction mechanism up to a remarkably high temperature.

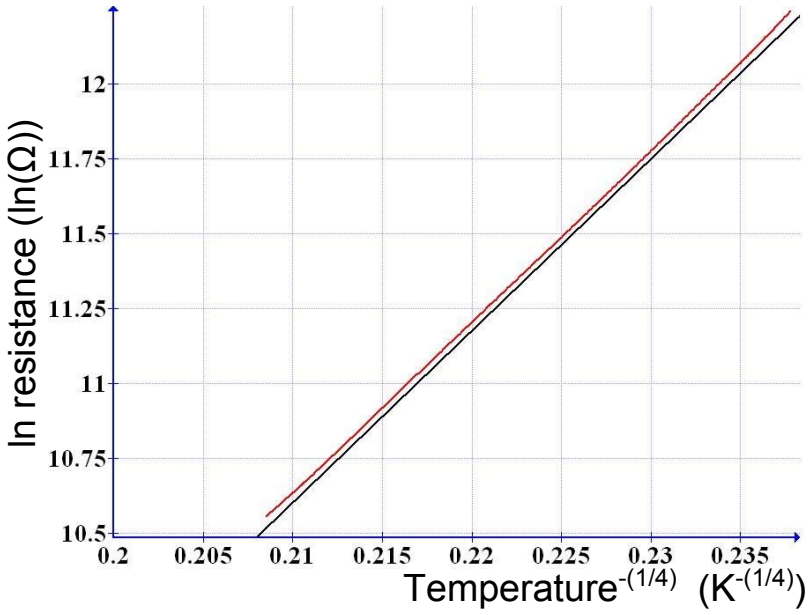

Figure 21: The natural logarithm of resistance versus the inverse fourth root of temperature, for a sample structure on alumina heated to 520 K. Straight black line is added as a guide to the eye.

More accurate fitting was obtained for the variation of the model parameters and respective comparison between the behaviour of the different substrates. The parameters of the variable range hopping model, B and A, are found to be 63 ± 1 $K^{-1/4}$

and 0.06 $\pm$0.01 $\Omega_{\square}$, respectively on alumina substrate structures. The large variation in the latter parameter is associated with the variation of the resistance in different batches.

In comparison, the steel substrate parameter A was roughly 56 $K^{-1/4}$. Thus it is evident that the alumina samples are slightly more sensitive for the resistance change, which is likely to follow from the disturbing layer below the sensor on the insulating layer.

4.2.6 Structure variation

The variation of the model parameters is linked to the variation of the fabrication parameters between batches and the resistance variation caused by masking within the batches. These errors are computed by utilizing the data in the repeated experiments using the sheet resistivity ($\Omega_{\square}$). The sheet resistivity for these samples was measured to be around 940 k$\Omega_{\square}$. The resistance was found to have a standard deviation of roughly 5 % at room temperature measured from a single batch. Between batches the variation was found to be roughly tripled. Although the variation in resistance is rather large, the variation in the behaviour of temperature and resistance was found to be much smaller. The variation was calculated through the ratio of two resistances at two different temperatures and found to be considerably smaller.

The standard deviation in resistance measurements of these structures on aluminium oxide was measured to be roughly 5 % within the same batch and up to 14 % between different batches measured at room temperature. At temperature of 200 ℃ both deviations were smaller by roughly 1 %. This variation can partly be associated with the surface roughness of the substrate pressure level during deposition which affects the structure of the film. However, the finished device is likely to be calibrated near specific temperature and thus these variations are necessary only for defining the resistance at operating temperatures.

Another important variation is the one associated with the slope of the resistance-temperature curve rather than resistances at single points. There may exist deviation between the measurements and the model, additional to those associated with materials due to changes in humidity, heating and similar effects. The variation can be estimated by ratios of resistances at two different temperatures, as the resistance temperature curve is expected to be sufficiently similar, the ratio of two points should not possess significant variation. Two such ratios are considered for the same data as in the variation of the resistance. First we selected the extreme temperatures of 200 ℃ and 30 ℃. Secondly we chose temperatures taken from the stable heating process 180 ℃ and 100 ℃ . The ratio of extreme temperatures contained variations of 2.3 %, 1.8 % and 0.8 % between batches, within batches and for the different measurements of a single structure respectively. For the stable temperature range the variation was found to be roughly half of that calculated for the extremal ratios. Compared to the variation of resistances at single points, the much smaller variations in the ratios suggest that the resistance-temperature behaviour is much less affected by the variation of the resistance or the variation in the fabrication parameters.

4.3 Piezoresistivity

The piezoresistive effect caused by the external pressure was experimented on three samples with different fabrication parameters, namely S1-S3 from the same batch used in the heat treatment experiments. The piezoresistive behaviour was observed both on alumina and steel substrates. Although the resistance change caused by the forces applied in this work were around 0.1 % of the room temperature resistance being insignificant in samples used for the examining thermistor properties. The behaviour was also examined on a more elastic polymer substrate and found to be several orders of magnitudes larger, thus making the piezoresistive abilities of the fabricated films useful in other applications and limiting the temperature sensing with some substrates. Also the mechanical vibrations were studied and the respective effect on the sensor was estimated to be minimal.

Next, we consider the pressure testing experiment, in which a force was directed on a sample surface. Figure 22(a) illustrates the results for the sample S2. The figure describes the proportional change in resistance with respect to the force applied on the part of the sensor structure at room temperature. The force of one newton corresponds roughly to 50000 pascal pressure on the contact area, which is roughly one third of the whole area of the sensor. However, the alumina samples are rough, which can effectively decrease the area of contact.

The resistance change is roughly linear under the measured pressures, yet slight deviation is observed. This and the natural requirement of curve reaching origo when no pressure is applied suggest a different kind of dependency.

The power law fitting is illustrated in the figure. Also, the values with the low pressures were deemed to be more inaccurate as suggested in figure 22(b). The figure describes the rough derivative of the resistance against the force applied, with the standard deviation. Thus, it is also evident that after the initial change in resistance the further increase in pressure has a weaker effect.

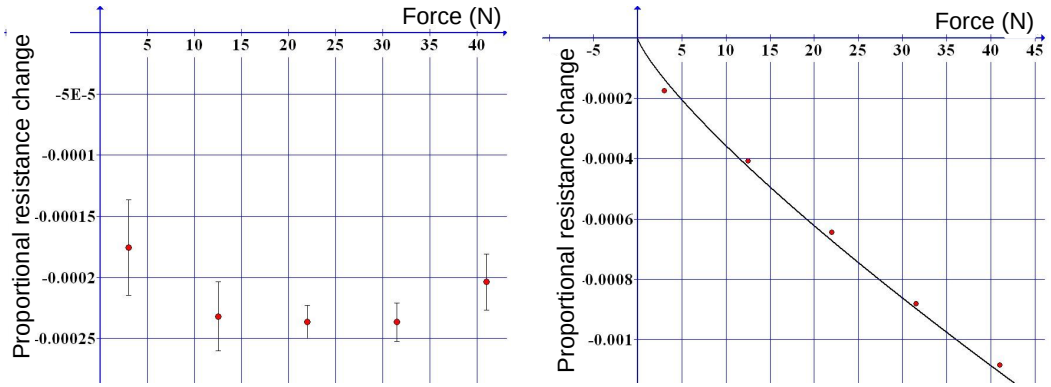

(a) (b)

Figure 22: The change of sensors resistance under applied force (a) and a rough derivative corresponding each added weight (b) for sample S2. Note that the first point corresponds to the shaft pressing the sensor, corresponding to smaller force increase than with later increments.

The effect for pressure on the whole sensor area is expected to follow linearly with the size of the area pressed. The pressed area is roughly one third of the whole sensor area, and the change when whole structure is under pressure would be roughly 0.3 % of the resistance at room temperature. Similar effect is presumed to occur at elevated temperatures, as the pressure essentially strains the structure in a manner that changes the resistance. The strain in the structure is almost independent of temperature, essentially because the material is aged and thus already relaxed. The increasing temperature causes an increase in the number of electrons contributing to conductivity. Though the strain would cause a similar effect in the material, the increased amount of conduction electrons causes pressure to have a proportionally smaller effect. The pressure effect has no significantly different behaviour that would be related to the fabrication parameters as suggested by figure 23 containing normalized results for all the samples.

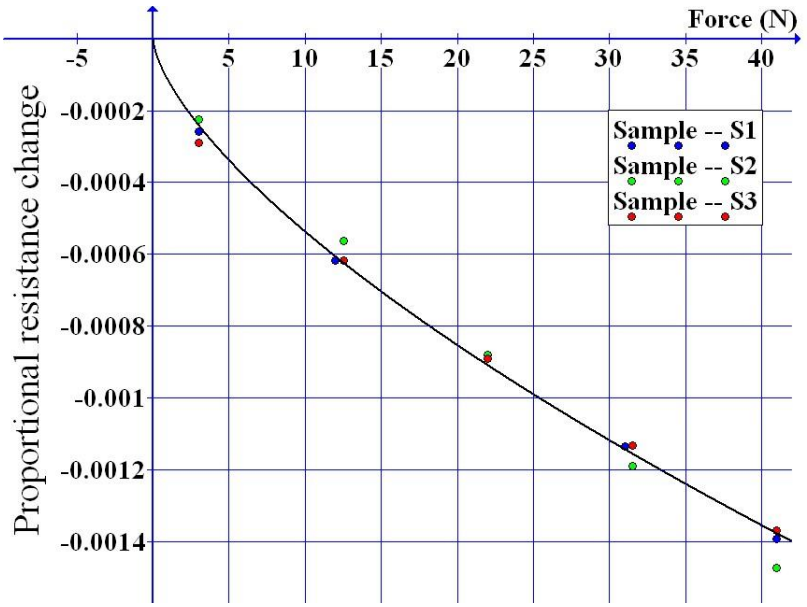

Figure 23: The comparison between the change of resistance with applied force observed as being proportional to the measured unburdened resistance.

These results for aluminium oxide indicate that the sensor resistance can be altered by external pressure. Yet, there were no results indicating any relation on the steel substrate, as the sensor resistance did not react to the applied pressure. No dependency was observed indicating that behaviour related to the sensor structure itself. However, the substrate and the insulating layer might cause these results. The substrate is much thicker than the alumina substrate and also has much smoother surface. With the thinner sensor film, these factors may result in weaker deformation and strain on the sensor structure by the external pressure.

The insulating layer was found to have an effect on the formation of a conducting layer below the sensor structure altering the behaviour. These in turn would cause even weaker effect on resistance, which would easily not be observed because of noise in the measurements. Finally, one concern is the possible effect of the measurement

head, a polyester tape, pressing the sensor surface. The nature of contact area may bring several unknown variables into the measurement, such as any conductive impurities or any humidity concentrated on the contact area. However, another experiment conducted for alumina clearly indicates that this dependency exists.

Several samples on a polyamide polymer substrate were fabricated, in order to obtain additional information of the possible limits of the resistance change induced by the external pressure. This much more elastic substrate allows greater deformation of the thin film structure and consequently a greater effect on resistance. The results for similar pressure experiment for polymer are illustrated in figure 24, note that the first point is the shaft with 1 kg weight. Significant increase in resistance change is obtained in comparison with the more rigid substrates. The maximal pressure on the polymer corresponds to 7 % change in the resistance, indicating an increase in sensitivity by almost two orders of magnitude. Also, there is no indication of the response being limited in the structure meaning even larger responses could be expected with further testing.

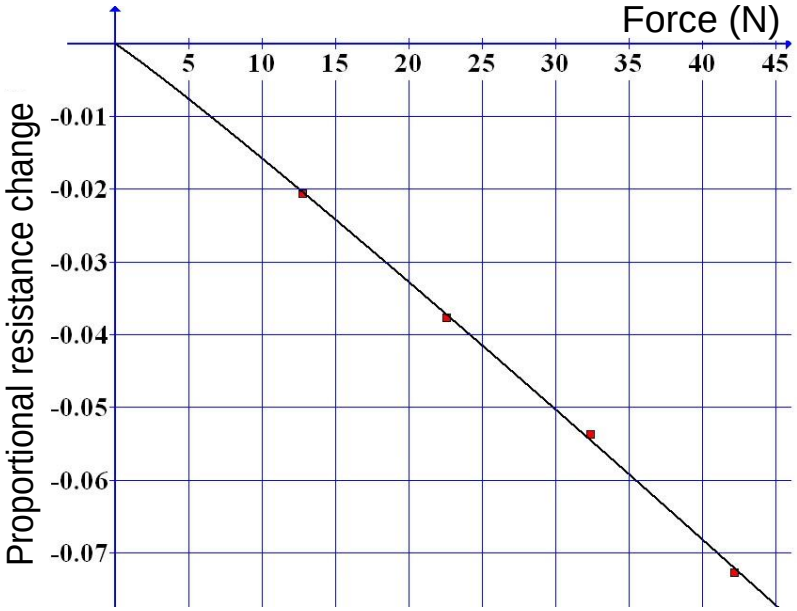

Figure 24: The change of sensors resistance on the polymer substrate corresponding to the external force directed on the sensor.

The one more experiment conducted for the measurement of the piezoresistance effects was the bending of the substrate to cause shear stress on the sensor structure. The experiment was conducted by bending the substrate in both viable directions and the results corresponding are shown in figure 25, with a linear fit. The figure shows the proportional change in resistance against the force used in bending, for one sample on alumina. The resistance change is actually negative, when the structure is on the opposite surface in comparison with the one where the force is directed (convex surface with respect to the sensor). The opposite changes result from the opposite shear stress compared to the sensor being on the concave surface.

Reasonably enough, the results show nearly linear increase in the resistance when

the force is increased as in the concave case, and decrease in the resistance on the convex case. The linearity is highly expected in this case as the aluminium oxide in the substrate is substantially rigid, bending only slightly even under large forces. As previously with the pressing experiment, the zero weight necessarily corresponds to zero change of resistance, thus power law should provide the more reasonable model. For samples fabricated with different parameters, there were no significant difference from the behaviour depicted by the figure 25. However, the slight difference observed between the directions of bending is present in all examined samples. The difference is likely to be related to the initial strain in the ta-C structure, thus the force increasing the strain differs in effect from the force opposing the initial strain.

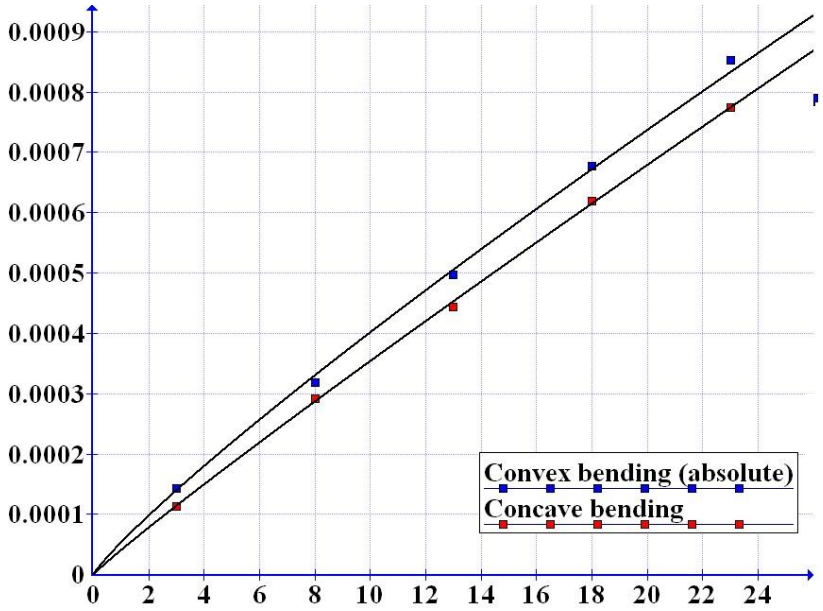

Figure 25: The change of resistance as a function of the applied bending force, respectively for the surface on which the sensor is located. In the convex surface, or bending, the sensor is located on the opposite side from the force directed on the substrate and vice versa.

In the end, the significant pressure on the sensor alters the resistance in the sensor structure by the maximum value of roughly 0.1 %. Note that, though the plastic structure possesses more sensitive behaviour it has not been considered as a substrate for thermistor. The effect of pressure scales with the sensor area subjected to the pressure and thus fabricating smaller structures would easily decrease the sensitivity to pressure. On the other hand, the steel substrate showed no noticeable dependency between resistance and pressure. On the contrary as the temperature changes by one degree, the resistance changes roughly by 1 % at room temperature, as determined in the previous section. Thus the error in the measured temperature is less than 0.1 degrees by the external pressure variation of less than 2 MPa.

Closely linked to the pressure is its frequent alteration, the mechanical vibration. The vibration might cause unwanted microphonical effects on the sensor resistance. However, this kind of effect was not observed when the sample sensor, P1, was com-

pared to a commercial resistor designed for low alteration of resistance by external conditions. The resistor and the sensor structure had resistances 1 MΩ and roughly 0.9 MΩ, respectively.

The figure 26 shows the graph of the standard deviation of the sensor and the resistor. Deviation has been calculated on thirty consequential measurements to neglect the sensor resistance changing with temperature. This approach also compensates the loss of accuracy as the measurement interval was roughly 0.14 seconds, whereas the vibration period corresponded to less than 0.1 seconds.

The beginning of the graph corresponds to a period of roughly two minutes, in which there are no vibrations present. With no vibration present the sensor possesses smaller deviation than the resistor. The smaller variation is likely to be caused by the bulkier form of the sensor on alumina substrate, being less affected by air flow and other environmental disturbance affecting wiring. As an important result for this thesis, it is already seen that microphonic effects do not cause significant error on the sensor resistance as the standard deviation of 50 Ω is proportionally less than 0.01 %. This is true only for the low frequency regime of roughly 10 Hz, thus further experiments with other sources should be examined.

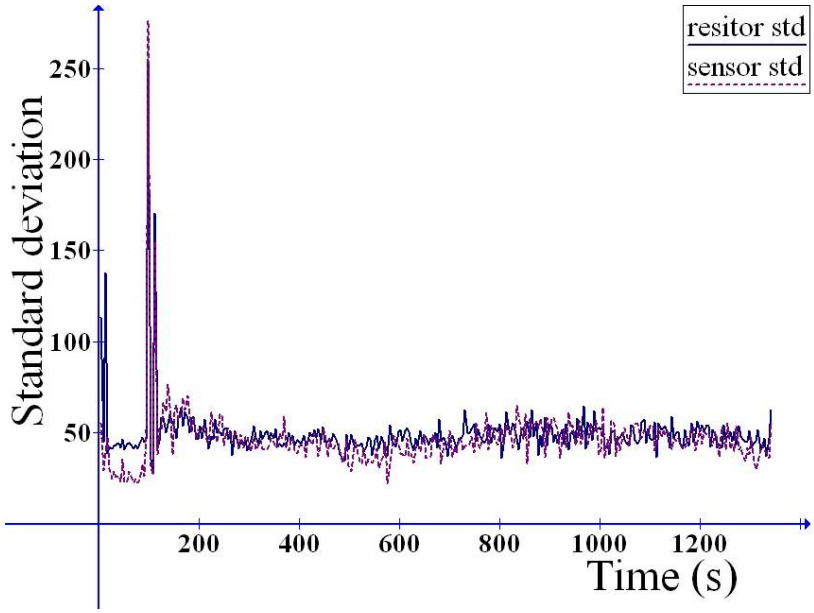

Figure 26: Standard deviation of the sensor and resistor resistance under mechanical vibration. No significant difference is seen during vibration, yet sensor varies slightly less on the beginning when vibration is not applied.

4.4 Titanium contacts

When considering the whole structure, the resistance of titanium contacts can cause unwanted disturbance in the output of the sensor. Thus the resistivity of titanium was explored by fabricating a set of thin and narrow titanium structures for four point measurement. The width of the titanium contacts examined varied from 120

microns to 1250 microns with a fixed length of 4 mm and thickness. Both aluminium oxide and silicon were used as substrates to describe the difference between roughness values and to avoid possible problems with insulating layer coated on a steel substrate. We found a clear difference with resistances between two substrates showing rather significant higher resistance on rougher surfaces. Furthermore, the junction of the titanium and the amorphous carbon film was examined and found to be ohmic.

The measured resistances of the structures are shown in figure 27. Both of the substrates show nonlinear change in resistance at low widths yet on alumina low width has clearly larger effect, likely caused by roughness of the surface. On larger widths both substrates show linear dependency between the resistance and the width of the contact. Similarly, to the observed effect with low line widths, the roughness of the alumina substrate is likely to cause the difference in the magnitudes of the resistance. The separation between the resistances on the substrates is roughly one order of magnitude on the largest widths.

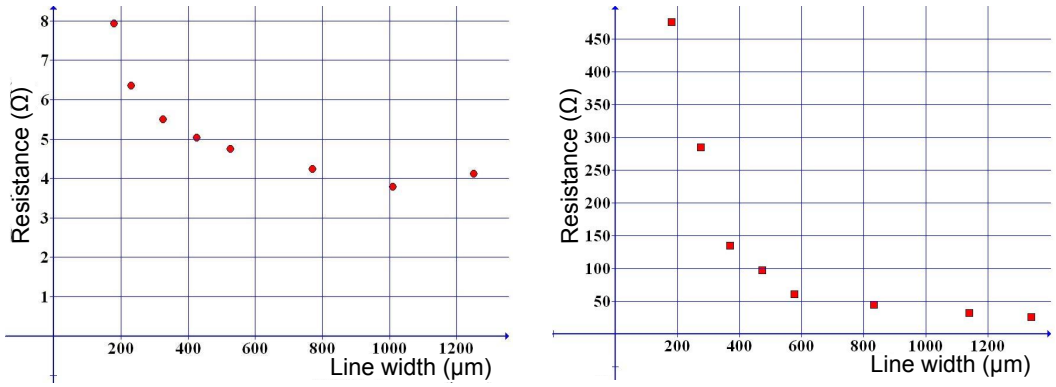

(a) (b)

Figure 27: The resistance of titanium on silicon (a) and alumina (b) with respect to the line width.

Sample contacts on the aluminium oxide were heated to 400 ℃ temperature to measure possible permanent effect of the temperature on the titanium contact. The annealing caused titanium to change in colour, from metallic grey to gold, which is assumed to be associated with titanium absorbing nitrogen from air (as TiN films fabricated tend to possess similar colouring). However, no major change with resistivity was observed, thus titanium contacts can withstand the temperatures better than ta-C sensor structures on alumina.

Another interest with the titanium contact would be the nature of junction with ta-C structure. As ta-C is a semiconductor, the junction might cause problems when having a Schottky junction instead of an ohmic contact. Former results in a diode like behaviour of the structure, whereas the latter would be strictly linear. Figure 28 contains the voltage-current relationship of a typical sensor structure experimented in this thesis. These structures are essentially metal-semiconductor-metal structures, thus the diode like behaviour would be observed regardless the direction of current

and only the positive voltages are thus measured. Having a linear dependency between the applied voltage and resulting current clearly indicates that the contact between titanium and ta-C is an ohmic one.

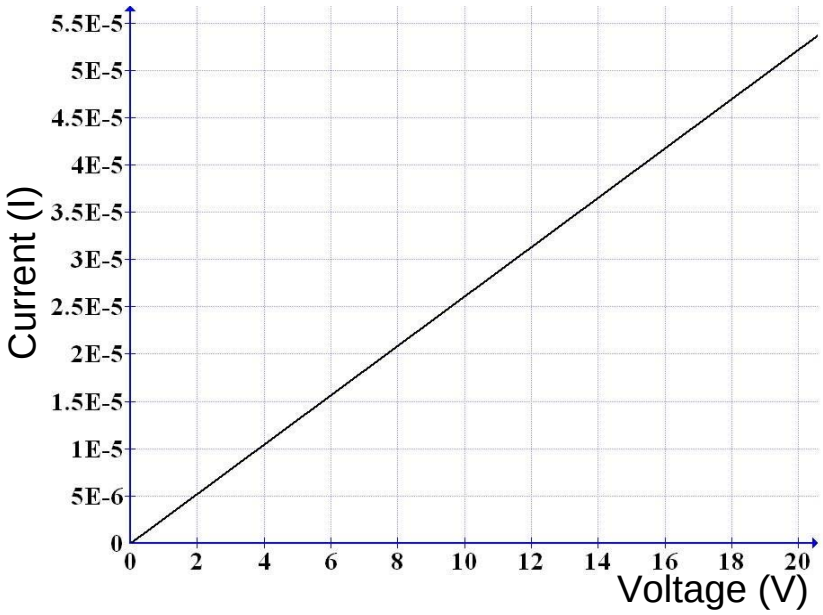

Figure 28: The voltage-current curve of the titanium–ta-C–titanium structure. This proves the ohmic nature of junction between the materials.

The titanium pads were also studied for several methods of contacting the wiring to the sensor. For the measurements in this thesis, the contact wiring to the titanium pads was mainly mechanical for heating experiments. Alternatively, electrically conducting adhesive was used for temperatures below 120 ℃ and pressure and other room temperature measurements. This limits the temperature range of the measurements below the designated temperature of roughly 200 ℃, though might be a viable solution in other applications. The mechanical contacts can be considered if the structure is embedded on a tool or similar piece, yet the mechanical contacts could cause some additional problems.

Additionally, the ultrasonic bonding of thin aluminium wire on the titanium pad was inspected as an alternative for the contacts. The alumina substrate was deemed too rough for the ultrasonic contacts as the rough surface did not provide sufficient area for good adhesion onto thin titanium pad. Another issue would be the bonding through the titanium pad and directly contacting to the sensor structure, or bypassing through the insulating layer. The former would result in Schottky contact between aluminium and amorphous carbon, though surrounding titanium pad would reduce the effect. The latter is very unlikely as the titanium pad itself is considerably thick to prevent the contact through it.

4.5 Insulating layer

Also, an insufficient insulating layer on the steel substrate might cause undesirable effects. The layer might contain cavities through the layer, or metallic particles reaching the surface while being created during the fabrication process. Thus the probability overlapping such a cavity or particle must be considered when fabricating contacts. On the other hand, the ta-C sensor structure has relatively high resistance and is not expected to be affected as the resistance would be reasonably high on such contacts. Thus, the main concerns are caused by the substrate contacts of the titanium pads in a way that the sensor is entirely bypassed. Sufficient insulating layer was found and several other alternatives were also considered promising.

In total, four different insulating layers, I1–I4, were inspected for suitability, primarily in terms of insulating properties. To this end, the layer I3, metal oxide, was selected for tests conducted on the steel substrate. The layer was an externally provided aluminium oxide magnesium oxide composition, which after polishing provided excellent insulation. However, this layer was also the thickest one and thus such behaviour was well expected.

The other insulating layers considered were aluminium oxide layer I2 and two other layers fabricated with DIARC FCAD method, layers I1 and I4. The main problem with these other layers, was the appearance of cavities reaching until to the substrate, which were more common on these radically thinner layers. With the I1 layer these cavities were too densely located on the surface to provide any real insulation between the substrate and the fabricated titanium squares. The externally provided I2 sample layer also possessed too high amount of cavities, with roughly one fifth of 1 mm^2 titanium pads were contacted. The final sample, I4, was fabricated with additional phases. These ones eventually resulted in less than 10 % of the 1 mm^2 titanium pads being connected, yet having only slight improvement compared to the sample I2. In addition, I4 was the thinnest sample experimented, thus being very promising candidate, yet as such the resistance through the layer itself needs to be increased from roughly 10 kΩ with 1 mm^2 pads.

4.6 Protective coating and adhesion between layers

In this section, adhesion between different structural layers and the effects of a protective coating on the sensor behaviour are discussed. For embedding the sensor to any mechanical, or similar tool it needs to be able to withstand external forces without breaking. In this aspect, the adhesion of the layers is a crucial matter. This section shows that no major issues with the adhesion of the layers were observed. Also as the protective coating provides a further protection against wear due to thermal and mechanical forces, it can alter the behaviour of the sensor. Yet no change was observed with the samples on which the protective coating was applied.

First, the attention is directed on the adhesion of the layers necessary for the sensor operation on different substrates. The alumina substrate was sufficiently good for adhesion of the sensor layers, both the titanium contacts and amorphous carbon sensor itself. We anyway observed flaking of the amorphous carbon sensor

when annealed to temperatures around 350 ℃. As the structures were sufficiently thin and as fabricated by the familiar method, the surfaces remain rough and thus maintained good adhesion of successive layers. For the protective coating there were no adhesion problems with the other layers, nor the combined structure caused breaking of the contacts.

For the steel substrate and different insulating layers, rather good but slightly varying adhesion was achieved. The insulating magnesium-aluminium oxide layer required an additional fabrication phase, which resulted in good adhesion for amorphous carbon sensor. The masking caused the edges of the pattern to break off. The breaking additionally resulted in partially poor adhesion of the titanium contacts, which partially overlapped the remains of poorly adhered carbon edges. Otherwise the adhesion of titanium was excellent with all tested insulating layers.

Thus the adhesion was found good for majority of the samples, though there is still room for improvement. The main concerns are related to the steel substrate with the studied insulating layer. To obtain sufficient adhesion the substrate was found to form one extra layer below the fabricated ta-C structure, which affected the properties of the sensor.

The possible changes in the behaviour resulted from the protective coating. On the alumina substrate noticeable changes were observed directly in the resistance or the temperature behaviour of the sensor structure when annealed proir to fabricating the protective layer. The annealing of the sample, with protective coating fabricated before ageing up to 250 ℃ neither resulted in any observable difference from the described behaviour between resistance and the temperature. However, one more general issue exists as the protective layer of ta-C contains significant amount of cavities as discussed with insulating layers. As a result, the sensor can be contacted through the protective layer, which might result in erroneous behaviour. However, the contact can be considered insignificant in the majority of applications, as there is no fabricated layer on top of the protective coating. Thus, any possible disturbing contact on the layer is better insulated from the sensor, resulting in considerably smaller effect.

5 Conclusions

In essence, the thesis successfully describes the amorphous carbon as a material possessing thermistor properties. These properties include the hysteresis of the material, repeatability of the measurements, the model for the resistance-temperature behaviour and the error related to the structure itself. Though there is certainly more work to be done on expanding the temperature range for the sensor operation, and in inspecting the accuracy of the structure more thoroughly and planning an actual device. The structures were fabricated on alumina substrate, as well as on a steel substrate with insulating layer, while maintaining the thermistor properties. The structure was additionally found to be sensitive to pressure, which effect on thermistor was limited by the rigidity of substrates. Also, the properties regarding the other parts of the device fabricated were inspected. These ones were the titanium contacts, insulating layers and the wear resistant layer protecting the surface. The actual protective quality of this layer was not tested in this thesis.

There were only a few issues regarding the fabrication of the samples. The masking, experimented also in this thesis, resulted in some adhesion issues with rougher alumina substrate even though, the difference in accuracy between different methods was not significant, and all the methods were considered sufficient for fabricating the structures.

In general, the adhesion of the structures was found sufficiently good with all the samples and layers fabricated. However, the achieved adhesion on the insulating layer of the steel substrates resulted in the appearance of a disturbing layer below the sensor structure. Further study should be made in order to minimize the presence of the disturbance in this particular situation, in order to prevent disturbing effects on the thermistor.

The amorphous carbon structures were found to exhibit thermistor properties, by following the model of hopping conductivity at least until 250 ℃, after annealing in a 50 ℃ higher temperature. The treatment was considered sufficient to stabilise material for the measurements on the lower temperature range. The aged amorphous carbon thermistor was found to lead to good repeatability with an error estimated to be less than 0.5 ℃ around the temperature of 200 ℃. And also observed to possess minimal error during cycling around the measured temperature range.

Perhaps of more interest was the piezoresistive behaviour found in the structure, examined by pressing the surface of the sensor or by bending the whole substrate. The piezoresistive behaviour was mostly studied as a source of error in the measurements of temperature in cases with changing pressure. The structures on alumina oxide were found to have roughly 0.1 % change in resistance as a result of 40 N force on area of roughly 20 mm^2. This pressure would result in roughly 0.1 ℃ error in the measured temperature. For the steel substrate there was no pressure dependency of the resistance, which was assumed to be unobservable due to the layer formed below the sensor. This assumption certainly needs to be confirmed, through fabrication of a sample with minimal effect from such a layer. In addition, the less rigid polymer substrate illustrated the potential of the amorphous carbon layer as a pressure sensing material. The microphonic behaviour of the structure was also studied in

relation to the error caused by external pressure. No effect was found in the sensor structure, when compared with the conventional resistor simultaneously observed.

The titanium pads were examined as contacts for the amorphous carbon structure. The ohmic contact with carbon and carbide forming titanium was confirmed in this thesis. Also, the resistivity of the contacts on the different substrates were examined to calculate the level of resistance of these contacts.

Furthermore, the different insulting layers were examined for the possibility of making contacts between the titanium pads and the steel substrate. One thick layer with good insulation was found along with two promising alternatives which might function after additional development.

Finally, a wear resistant amorphous carbon coating was fabricated over the sensor structures on the alumina substrate. The protective layer did not cause any effect on the sensor structure, had no problems with the adhesion nor broke the structure due to inherent stress in the fabricated amorphous carbon films.

6 Outlook

In this thesis we discuss the properties of the specific fabricated amorphous carbon structure as a thermistor. In addition, the pressure was found to have an observable effect on the resistance of the structure. The insulating layers, especially the promising thin film layers, are also of major interest for the further study. These three parts are the major points regardless the actual goal placed in this thesis.

The thermistor properties of amorphous carbon were observed, however, the equipment and samples used in the measurements were somewhat bulky for accurate measurements. Thus, a more faster responsive, smaller structure should be fabricated and studied in a more accurately controlled atmosphere. This would improve the rather crude accuracy of the thermistor and make comparison with other temperature measuring devices more reasonable. Other aspects, which should be studied, are the temperature limits, and activation energies, of the fabricated amorphous carbon material. The inspection of activation to the extended states conduction would require solving the issue of the film breaking during annealing temperature around of 350 ℃. Though, the upper limit is likely to be set around the oxidation temperature of carbon located above 450 ℃.

The most interesting result of this thesis is considered to be the pressure sensing capabilities of the amorphous carbon structure. The piezoresistive capability is clearly observed with the experiment conducted with polymer substrate, which resulted in a major alteration of the structure resistance. Thus the amorphous carbon film can function as a pressure or tension sensing device, as one can suggest based on the bending experiments. The piezoresistivity is combined with the good physical properties of amorphous carbon that enables the use in wide variety of application.

To this end, more experiments need to be conducted by placing the amorphous carbon structure under a variety of different mechanical forces. The experiments of this thesis merely introduced the microphonical property and evaluated the possible effect on the temperature measurements in limited fashion. Two cases would be of particular interest. The first one is the behaviour of the sensor under changes of surrounding pressure, that is the behaviour in high pressures or in a vacuum. Secondly, a more thorough inspection of vibrational properties of the amorphous carbon film should be performed. The microphonical experiment in this thesis was fairly limited as experimented at single and low frequency.

Thirdly, more notable point of interest is the fabrication of insulating thin films. Though one good solution was found for the fabrication of sensor structures on the steel substrate, the thickness of the layer in question was significant compared to the second alternative. A good thin insulating layer would be necessary for applications, which cannot tolerate major changes in the physical measures. Thus the insulating layer fabricated with the DIARC FCAD method could provide an excellent solution for such applications, after some effort directed on the improvement of the layer.

References

[1] J. Robertson. Diamond-like amorphous carbon. *Materials Science and Engineering: R: Reports*, 37(4-6), 2002.

[2] S. N. Mott. Electrons in glass. *Reviews of Modern Physics*, 50(2):203–208, 1978.

[3] J. Robertson and C. A. Davis. Nitrogen doping of tetrahedral amorphous carbon. *Diamond and Related Materials*, 4(4):441–444, 1995.

[4] G. Lazar, K. Zellama, M. Clin, and C. Godet. Band tail hopping conduction mechanism in highly conductive amorphous carbon nitride thin films. *Applied Physics Letters*, 85(25):6176–6178, 2004.

[5] X. Shi, H. Fu, J. R. Shi, L. K. Cheah, B. K. Tay, and P. Hui. Electronic transport properties of nitrogen doped amorphous carbon films deposited by the filtered cathodic vacuum arc technique. *Journal of Physics Condensed Matter*, 10(41):9293–9302, 1998.

[6] C. Godet. Electronic localization and bandtail hopping charge transport. *Physica Status Solidi (B) Basic Research*, 231(2):499–511, 2002.

[7] W. S. Williams. Transition metal carbides, nitrides, and borides for electronic applications. *JOM*, 49(3):38–42, 1997.

[8] F. M. Wang, M. W. Chen, and Q. B. Lai. Metallic contacts to nitrogen and boron doped diamond-like carbon films. *Thin Solid Films*, 518(12):3332–3336, 2010.

[9] J. Robertson. Improving the properties of diamond-like carbon. *Diamond and Related Materials*, 12(2):79–84, 2003.

[10] J. D. Carey and S. R. P. Silva. Disorder, clustering, and localization effects in amorphous carbon. *Physical Review B - Condensed Matter and Materials Physics*, 70(23):1–8, 2004.

[11] G. Fanchini, S. C. Ray, and A. Tagliaferro. Density of electronic states in amorphous carbons. *Diamond and Related Materials*, 12(3-7):891–899, 2003.

[12] V. S. Veerasamy, G. A. J. Amaratunga, C. A. Davis, A. E. Timbs, W. I. Milne, and D. R. McKenzie. N-type doping of highly tetrahedral diamond-like amorphous carbon. *Journal of Physics: Condensed Matter*, 5(13):L169–L174, 1993.

[13] B. Kleinsorge, A. Ilie, M. Chhowalla, W. Fukarek, W. I. Milne, and J. Robertson. Electrical and optical properties of boronated tetrahedrally bonded amorphous carbon (ta-c:b). *Diamond and Related Materials*, 7(2-5):472–476, 1998.

[14] V. S. Veerasamy, J. Yuan, G. A. J. Amaratunga, W. I. Milne, K. W. R. Gilkes, M. Weiler, and L. M. Brown. Nitrogen doping of highly tetrahedral amorphous carbon. *Physical Review B*, 48(24):17954–17959, 1993.

[15] B. Kleinsorge, A. C. Ferrari, J. Robertson, and W. I. Milne. Influence of nitrogen and temperature on the deposition of tetrahedrally bonded amorphous carbon. *Journal of Applied Physics*, 88(2):1149–1157, 2000.

[16] O. S. Panwar, M. A. Khan, B. S. Satyanarayana, S. Kumar, and Ishpal. Properties of boron and phosphorous incorporated tetrahedral amorphous carbon films grown using filtered cathodic vacuum arc process. *Applied Surface Science*, 256(13):4383–4390, 2010.

[17] G. A. J. Amaratunga, J. Robertson, V. S. Veerasamy, W. I. Milne, and D. R. McKenzie. Gap states, doping and bonding in tetrahedral amorphous carbon. *Diamond and Related Materials*, 4(5-6):637–640, 1995.

[18] P. Stumm, D. A. Drabold, and P. A. Fedders. Defects, doping, and conduction mechanisms in nitrogen-doped tetrahedral amorphous carbon. *Journal of Applied Physics*, 81(3):1289–1295, 1997.

[19] P. K. Sitch, G. Jungnickel, T. Köhler, T. Frauenheim, and D. Porezag. p- and n-type doping in carbon modifications. *Journal of Non-Crystalline Solids*, 227-230(PART 1):607–611, 1998.

[20] C. W. Chen and J. Robertson. Doping mechanism in tetrahedral amorphous carbon. *Carbon*, 37(5):839–842, 1999.

[21] D. R. McKenzie. Tetrahedral bonding in amorphous carbon. *Reports on Progress in Physics*, 59(12):1611–1664, 1996.

[22] A. C. Ferrari, B. Kleinsorge, N. A. Morrison, A. Hart, V. Stolojan, and J. Robertson. Stress reduction and bond stability during thermal annealing of tetrahedral amorphous carbon. *Journal of Applied Physics*, 85(10):7191–7197, 1999.

[23] M. M. M. Bilek and D. R. McKenzie. A comprehensive model of stress generation and relief processes in thin films deposited with energetic ions. *Surface and Coatings Technology*, 200(14-15):4345–4354, 2006.

[24] D. G. McCulloch and A. R. Merchant. The effect of annealing on the structure of cathodic arc deposited amorphous carbon nitride films. *Thin Solid Films*, 290-291:99–102, 1996.

[25] N. M. J. Conway, A. C. Ferrari, A. J. Flewitt, J. Robertson, W. I. Milne, A. Tagliaferro, and W. Beyer. Defect and disorder reduction by annealing in hydrogenated tetrahedral amorphous carbon. *Diamond and Related Materials*, 9(3):765–770, 2000.

[26] D. G. McCulloch, J. L. Peng, D. R. McKenzie, S. P. Lau, D. Sheeja, and B. K. Tay. Mechanisms for the behavior of carbon films during annealing. *Physical Review B - Condensed Matter and Materials Physics*, 70(8):085406–1–085406–8, 2004.

[27] A. Tibrewala, E. Peiner, R. Bandorf, S. Biehl, and H. Lüthje. Transport and optical properties of amorphous carbon and hydrogenated amorphous carbon films. *Applied Surface Science*, 252(15):5387–5390, 2006.